Integration of moisture transfer through walls into an urban climate model and application to the medieval city centre of Cahors (France)

Margot Ruiz, Valéry Masson, Marion Bonhomme, Marina Malagoni de Almeida, Stéphane Ginestet

Integration of moisture transfer through walls into an urban climate model and application to the medieval city centre of Cahors (France)

Margot Ruiz[a,b] *, Valéry Masson [b] , Marion Bonhomme [a], Marina Malagoli [a,c], Stéphane Ginestet [a]

[a] LMDC, Université de Toulouse, INSA, UPS, Toulouse, France

[b] CNRM, Université de Toulouse, Météo-France, CNRS, Toulouse, France

[c] Instituto Federal de Goiás, Goiás, Brasil

* Corresponding author: 135 Avenue de Rangueil, 31400 Toulouse, France.

E-mail address: mruiz@insa-toulouse.fr (M. Ruiz)

Integration of moisture transfer through walls into an urban climate model and application to the medieval city centre of Cahors (France)

Margot Ruiz[a,b] *, Valéry Masson [b] , Marion Bonhomme [a], Marina Malagoli [a,c], Stéphane Ginestet [a]

[a] LMDC, Université de Toulouse, INSA, UPS, Toulouse, France

[b] CNRM, Université de Toulouse, Météo-France, CNRS, Toulouse, France

[c] Instituto Federal de Goiás, Goiás, Brasil

* Corresponding author: 135 Avenue de Rangueil, 31400 Toulouse, France.

E-mail address: mruiz@insa-toulouse.fr (M. Ruiz)

Abstract

Moisture transfer is a key phenomenon for simulating the energy balance of the walls of historical buildings as it has an impact on indoor and outdoor comfort, energy consumption and the durability of the walls. It is therefore essential to consider moisture transfer through walls when simulating old city centres. However, urban climate models neglect this phenomenon. The objective of this paper is to integrate the coupled mass and heat transfers into the urban climate model Town Energy Balance (TEB). A specially designed numerical method for solving hygrothermal transfers at the urban scale is updated and the hygrothermal transfer through walls is integrated into TEB. The reliability of this modified version of TEB for representing a historical district is verified by comparing the simulated results with in-situ measurements in a building of the medieval city centre of Cahors (France). The comparison is carried out for several points in the wall and for indoor conditions. The integration of the moisture transfers through the walls greatly improves the moisture estimation inside the building. This new version of the model gives a good representation of the hygrothermal behaviour of a historical building and could therefore be used to compare several renovation scenarios.

Keywords:

Hygrothermal behaviour, urban climate model, historical city centre, in-situ measurement

1. Introduction

Given the climate emergency, enhancing building energy efficiency is a priority. This is particularly true in historical city centres, which are composed of poorly insulated buildings. In addition, their complex urban forms make them particularly vulnerable to Urban Heat Island (UHI) phenomena (Rosso et al., 2018), expressed by the observation of higher temperatures in cities than in the surrounding urban areas (Oke, 1988). Research projects have shown that building retrofit is a major lever for limiting the UHI effect (Masson et al., 2014, 2013). Historical city centres are often subject to constraints related to heritage preservation. For example, a retrofit of historical walls by applying external insulation is not possible (Hansen et al., 2018). According to Cassar (2009), two major challenges to be confronted in the 21st century are the urgency of energy renovation and the conservation of historical heritage.

Building energy simulation is an effective method for evaluating the retrofitting of historical city centres. It allows easy comparison of different strategies and predictions of building and wall behaviour in different configurations, over long timescales and in various climates (current or future) (Akkurt et al., 2020; Webb, 2017). However, existing tools for energy simulation at the building or city scale are designed to represent modern buildings. The thermal properties of historical buildings are very different from those of more recent buildings (Camuffo, 2019; Cantin et al., 2010). Webb (2017) highlights two main limitations of BES (Building Energy Simulation) models for representing old buildings. The first is that the standard assumptions made about the input data are not appropriate. The second limitation is that these tools do not adequately model certain physical phenomena, such as moisture exchange at the wall level. This phenomenon is particularly important in the case of historical centres. It has a strong impact on the durability of old walls (Hansen et al., 2018; Harrestrup and Svendsen, 2016; Straube and Schumacher, 2007). In addition, the rain and moisture buffering capacity of materials can have a considerable effect on energy consumption, and indoor and outdoor comfort in certain configurations (Abuku et al., 2009; Maalouf et al., 2014; Osanyintola and Simonson, 2006; Saneinejad et al., 2014, 2012; Zhang et al., 2017, p. 2; Zhou et al., 2020).

Some BES tools perform whole-building hygrothermal simulations (Carmeliet et al., 2011; Rode and Grau, 2003; Woloszyn and Rode, 2008); they use various approaches with different levels of accuracy and computational costs (Janssens et al., 2008). However, to the best of our knowledge, no simulation tool on an urban scale is currently able to model the coupled heat and mass transfer through walls, under realistic weather conditions and on large spatio-temporal scales. A method has been developed specifically to facilitate their integration into an urban scale model but it has not yet been implemented into an urban climate tool (Ruiz et al., 2023).

This study employs the Town Energy Balance (TEB) model designed to parametrise energy, radiative, water and turbulent exchanges between built surfaces and the atmosphere (Masson, 2000). This tool is also used to assess the microclimate in the street and to simulate the energy balance of buildings (Bueno

et al., 2012). A neighbourhood is represented with simplified geometry, which means that buildings are not modelled individually. Thus, urban climate models, such as TEB, can simulate large spatial scales (from the neighbourhood to the agglomeration), over long time periods. The use of an urban climate model for building energy simulation allows the following two key phenomena to be taken into account: (1) the strong influence of the urban microclimate on boundary conditions of façades (Dorer et al., 2013) and (2) the impact of waste heat from HVAC equipment and buildings on the urban microclimate (Yang et al., 2017).

In this paper, an application is made on the medieval city centre of Cahors (France), which is subject to heritage conservation regulations. In the framework of the ENERPAT project, a living-lab approach was set up, with the aim of promoting an appropriate and suitable renovation of the old walls, as well as revitalising the old centre and bringing back the population (Claude et al., 2017). Several buildings have been retrofitted using hemp-lime insulation and long-term monitoring has been set up (Claude, 2018; Claude et al., 2019, 2017; Malagoni de Almeida, 2022).

The objective of this paper is to integrate the moisture transfer through walls in the urban climate model TEB. The urban model thus modified will allow to consider the two main characteristics of old city centres: their very dense urban form and the hygrothermal performance of the walls (Claude et al., 2019). Section 2 presents a model of coupled mass and heat transfer through walls and a numerical solution method specially adapted to the urban scale. In section 3, this numerical method is used to integrate the moisture transfer through walls in the urban climate model TEB. Section 4 presents the medieval city centre of Cahors and its modelling using the TEB tool. This section also discusses the reliability of the model and the impact of moisture transfer, based on a comparison of in-situ measurements and results simulated by TEB before and after integration.

2. Numerical method for solving hygrothermal transfer at the urban scale

Currently, the urban climate model TEB only takes account of heat transfer by thermal conduction through the walls and neglects the influence of water in liquid and vapour form on the wall behaviour. The objective of this work is to integrate the moisture transfers through walls. However, the most common methods of numerical solution of coupled transfers are not suitable for the urban climate model. Adaptations have to be made on the space-time discretization scales and on the numerical resolution scheme. Explicit discretization schemes are difficult to integrate in TEB, while implicit schemes require the use of complex, iterative solving methods. Implicit methods are generally based on a variable timestep depending on convergence, which makes them complicated to integrate into a fixed timestep urban model. For these reasons, a numerical method has been specially developed by Ruiz et al. (2023) to work at the urban scale. This method will be used as a basis for the present work. Some modifications have been introduced to make the method even more easily integrable in TEB and more

robust for numerical stability in the case of dynamic boundary condition calculations. The changes made are detailed in this section.

2.1. Coupled heat and mass transfer model

The model to be integrated into TEB describes the hygrothermal transfers through a multilayer wall, in 1D. It considers the main phenomena of moisture and heat transfer. It models thermal conduction, water vapour transfer through Fick's diffusion, and liquid water transport by applying Darcy's law. It is based on the same assumptions as the work of Ruiz et al. (2023), i.e. it neglects: the Soret effect, the effect of gravity in the pores, the influence of temperature on moisture storage, the contribution of the gas phase to heat storage, the transfer of air through the wall, ice formation, pore weathering processes, chemical reactions and the effect of hysteresis. In addition to these simplifications, two new assumptions are made, neglecting: the dependence of heat storage on the variation of moisture storage, and the effect of liquid water transfers on the heat equation (Mendes et al., 2003).

Applying these assumptions and using temperature and capillary pressure as the driving potentials, the energy and mass conservation balances are written as follows:

$$(c_{mat}\,\rho_{mat} + c_l\,w)\frac{\partial T}{\partial t} = \frac{\partial}{\partial x}\left(\left(\lambda + L_v K_v\left[\frac{\partial p_{v,sat}}{\partial T}\varphi + \frac{p_c}{T}\frac{\rho_v}{\rho_l}\right]\right)\frac{\partial T}{\partial x} + \left[c_l(T - T_{ref})K_l + L_v K_v\frac{\rho_v}{\rho_l}\right]\frac{\partial p_c}{\partial x}\right) \quad (1)$$

$$\frac{\partial w}{\partial p_c}\frac{\partial p_c}{\partial t} = \frac{\partial}{\partial x}\left(K_v\left[\frac{\partial p_{v,sat}}{\partial T}\varphi + \frac{p_c}{T}\frac{\rho_v}{\rho_l}\right]\frac{\partial T}{\partial x} + \left[K_l + K_v\frac{\rho_v}{\rho_l}\right]\frac{\partial p_c}{\partial x}\right) \quad (2)$$

with c_{mat} the heat capacity of the material, ρ_{mat} the density of the material, c_l the heat capacity of liquid water *(J/K)*, w the liquid water content *($kg.m^{-3}$)*, h_l the liquid water enthalpy *(J)*, h_v the vapour enthalpy *(J)*, K_l the liquid conductivity *(s)*, p_c the capillary pressure *(Pa)*, p_v the vapour pressure *(Pa)*, K_v the vapour permeability of the material *($kg.m^{-1}.s^{-1}.Pa^{-1}$)*, c_v the heat capacity of water vapour *(J/K)*, T_{ref} the reference temperature *(K)*, φ *the relative humidity, and* L_v the heat of vaporization *($2500\ J.kg^{-1}$)*.

The boundary conditions represent the thermal (q_{s*} in $W.m^{-2}$) and mass (j_{s*}in $kg.m^{-2}.s^{-1}$) fluxes exchanged between the wall surface and its environment. Transfers at the external surface include thermal convection, mass convection, rain, diffuse and direct solar radiation, and long-wave radiation from the atmosphere and other surfaces of the urban environment. Boundary conditions at the interior surface are restricted to long-wave radiation, thermal and mass convection.

$$q_{sext} = h_{conv,th}\,(T_{ext} - T_{sext}) + \alpha q_{SW,inc} + q_{LW} + L_v h_{conv,m}\left[p_{v,ext} - p_{sat}(T_{sext})exp\left(\frac{p_{c,sext}}{\rho_l R_v T_{sext}}\right)\right] + c_l(T_{ext} - T_{ref})j_{rain} \quad (3)$$

$$j_{sext} = h_{conv,m}\left[p_{v,ext} - p_{sat}(T_{sext})exp\left(\frac{p_{c,sext}}{\rho_l R_v T_{sext}}\right)\right] + j_{rain} \quad (4)$$

$$q_{sint} = h_{conv,th}(T_{int} - T_{sint}) + L_v h_{conv,m}\left[p_{v,int} - p_{sat}(T_{sint})exp\left(\frac{p_{c,sint}}{\rho_l R_v T_{sint}}\right)\right] + q_{LW} \quad (5)$$

$$j_{sint} = h_{conv,m}\left[p_{v,int} - p_{sat}(T_{sint})exp\left(\frac{p_{c,sint}}{\rho_l R_v T_{sint}}\right)\right] \quad (6)$$

with $h_{conv,th}$ the convective heat coefficient $(W.m^{-2}.K^{-1})$, $h_{conv,m}$ the convective mass coefficient $(kg.m^{-2}.s^{-1}.Pa^{-1})$, α the absorption coefficient, $q_{SW,inc}$ the incident short-wave radiative flux $(W.m^{-2})$, q_{LW} the long-wave radiative flux $(W.m^{-2})$, and j_{rain} the wind-driven rain flow incident on the façade $(kg.m^{-2}.s^{-1})$.

2.2. Numerical method

The numerical solution method was specifically adapted to be easy to integrate into the TEB numerical scheme and to work at large spatio-temporal scales. The proposed method results from a compromise between the numerical methods generally used to solve coupled transfers and the simpler methods used to solve heat transfer through a wall in an urban climate model such as TEB, while taking account of the level of accuracy expected in an urban scale model (Ruiz et al., 2023). Indeed, TEB is already based on many assumptions such as that a neighbourhood is represented by a typical street and that only one wall composition is simulated per district.

The proposed method is based on an IMplicit/EXplicit discretization scheme (IMEX) (Gasparin et al., 2019). It has the advantage of being numerically stable and consistent, without using an iterative method for solving (Gasparin, 2019).

The time discretization implemented is five minutes (the typical timestep in TEB). This is reduced to ten seconds – only for the wall mass and thermal equations, not for all the TEB model – in the moments that are critical for convergence, thus ensuring the numerical stability of the model. To determine the critical moments for convergence, five tests are performed. They check for:

1. A large amount of rain absorbed by the wall,
2. Oscillations in temperatures or capillary pressures simulated on the interior and exterior surfaces,
3. A large variation rate for the temperature or the capillary pressure on the interior and exterior surfaces,
4. A large variation rate for the integrated water content,
5. The fact that capillary pressure does not become positive.

The procedure of the five tests is detailed in Ruiz et al. (2023). Only the test concerning oscillations has been modified. The new test not only observes the evolution of the sign of the variation rate, but also studies the evolution of the last two variation rates compared to the trend. This new procedure is detailed in **Fig. 1**, for capillary pressure at the outer surface. The same test procedure is applied to the capillary pressure at the inner surface, and to the simulated temperature at the inner and outer surfaces of the wall.

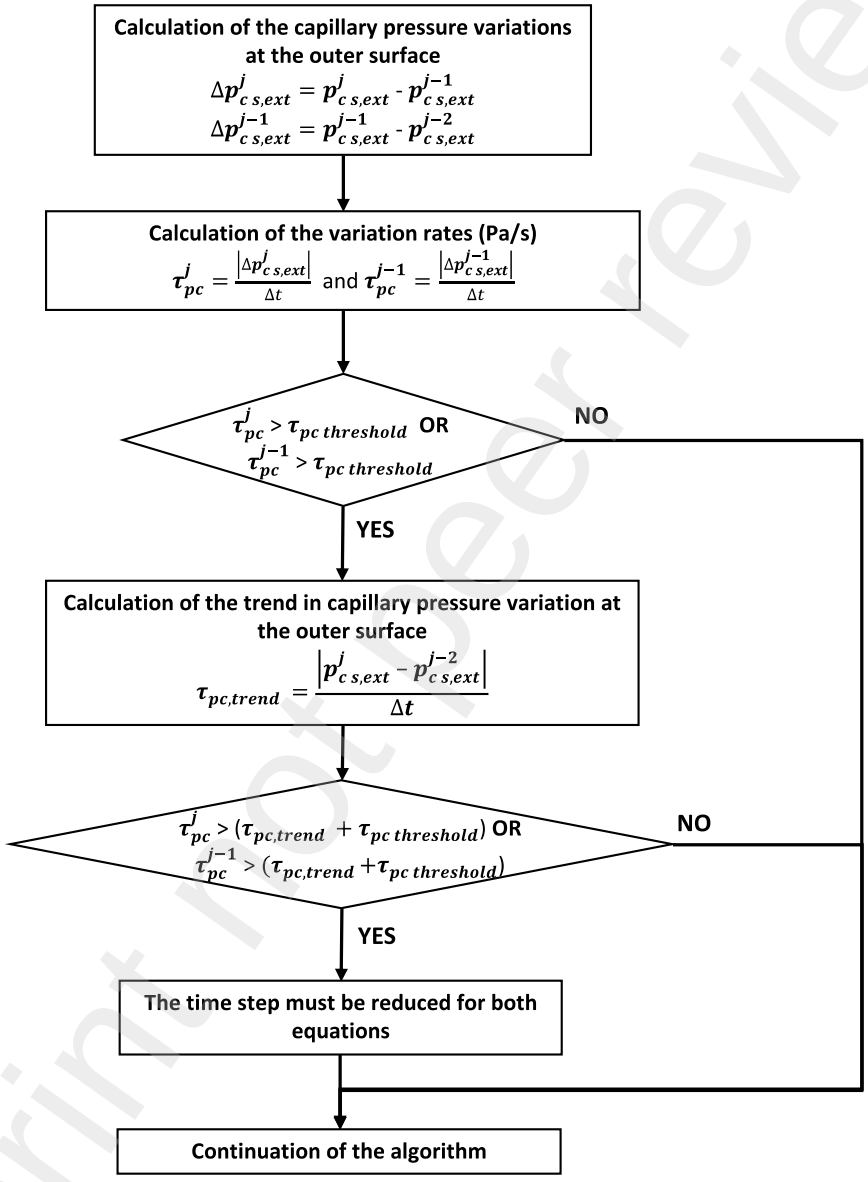

Fig. 1. Algorithm of Test 2 for capillary pressure at the exterior surface.

These tests are all governed by the threshold values summarised in **Table 1**, which were defined to represent acceptable thresholds and provide satisfactory results while limiting the number of timestep reductions. The definition of threshold values has been simplified in this new method: contrary to what takes place in Ruiz et al. (2023), a single set of threshold values allows numerical stability to be obtained for all the meshes.

One difference from previous work is that, if one of the tests provides unsatisfactory results, the timestep is decreased for both equations (mass and heat), in all cases.

Table 1
Threshold values for the five tests (modified from Ruiz et al. (2023).)

Test number	Variable	Units	Threshold values
Test 1	Absorbed rain rate	$kg.m^{-2}.s^{-1}$	0.00002
Test 2	Variation rate for		
	- Capillary pressure	$Pa.s^{-1}$	666.67
	- Temperature	$°C.s^{-1}$	0.000167
Test 3	Variation rate for		
	- Capillary pressure	$Pa.s^{-1}$	6666.67
	- Temperature	$°C.s^{-1}$	0.000667
Test 4	Variation rate for integrated water content	$kg.m^{-3}.s^{-1}$	0.000167
Test 5	Capillary pressure limit	Pa	0
	Replacement value for capillary pressure	Pa	-1e5

Concerning the spatial discretization, a constant, relatively coarse mesh has been chosen, in accordance with the result of the sensitivity analysis of Ruiz et al. (2023). The meshing technique used is based on a stretch factor of 1.5, a first mesh size of 0.001 m and a maximum mesh size of 0.1 m. There is no refinement of the mesh at the interface between two layers of different materials, as we are mostly interested in results on the external and internal surfaces of walls.

Finally, the numerical solution method used is the Lower-Upper (LU) decomposition method. This is also the method used in TEB for solving conductive heat transfer alone. It is possible to use this method because an IMEX discretisation scheme is implemented. It would not have been possible with a fully implicit scheme.

The numerical solution approach applied is a decoupled method, i.e. the mass equation and the heat equation are solved separately (by two separate matrix systems). Thus, the heat equation has only one unknown: the temperature, and the same is true for the mass equation, which determines the capillary pressure. The method presented in this paper solves the mass equation and then the heat equation. The first equation is used to calculate the capillary pressure at timestep *j+1*. Then, this value of the capillary pressure is used in the heat equation at timestep *j+1* (Fig**. 2**). This new approach makes it possible to solve both equations using the same amount of water at the same timestep. The results are therefore more consistent when the closure of the energy and mass balances are studied at the end of the timestep.

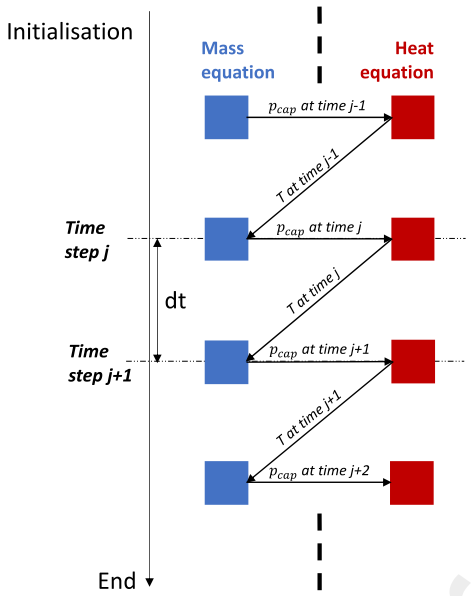

Fig. 2. Decoupled solution approach solving the mass equation and then the heat equation.

The following discretised mass and heat equations are used for solving at timestep *j+1* and at node *i*.

$$0 = (C_{PP})_i^j \frac{p_{c,i}^{j+1} - p_{c,i}^j}{\Delta t} + \left[\frac{(K_{PT})_{i-1/2}^j}{\Delta x_i}\frac{(T_i^j - T_{i-1}^j)}{\Delta x_{i-1/2}} - \frac{(K_{PT})_{i+1/2}^j}{\Delta x_i}\frac{(T_{i+1}^j - T_i^j)}{\Delta x_{i+1/2}}\right]$$
$$+ \left[\frac{(K_{PP})_{i-1/2}^j}{\Delta x_i}\frac{(p_{c,i}^{j+1} - p_{c,i-1}^{j+1})}{\Delta x_{i-1/2}} - \frac{(K_{PP})_{i+1/2}^j}{\Delta x_i}\frac{(p_{c,i+1}^{j+1} - p_{c,i}^{j+1})}{\Delta x_{i+1/2}}\right] \quad (7)$$

$$0 = (C_{TT})_i^j \frac{T_i^{j+1} - T_i^j}{\Delta t} + \left[\frac{(K_{TT})_{i-1/2}^j}{\Delta x_i}\frac{(T_i^{j+1} - T_{i-1}^{j+1})}{\Delta x_{i-1/2}} - \frac{(K_{TT})_{i+1/2}^j}{\Delta x_i}\frac{(T_{i+1}^{j+1} - T_i^{j+1})}{\Delta x_{i+1/2}}\right]$$
$$+ \left[\frac{(K_{TP})_{i-1/2}^j}{\Delta x_i}\frac{(p_{c,i}^{j+1} - p_{c,i-1}^{j+1})}{\Delta x_{i-1/2}} - \frac{(K_{TP})_{i+1/2}^j}{\Delta x_i}\frac{(p_{c,i+1}^{j+1} - p_{c,i}^{j+1})}{\Delta x_{i+1/2}}\right] \quad (8)$$

The coefficients of the matrices are written as follows:

$$C_{TT} = c_{mat}\,\rho_{mat} + c_l\,w;\; C_{PP} = \frac{dw}{dp_c};\; K_{TT} = \lambda + L_v K_{PT};\; K_{TP} = L_v K_v \frac{p_v}{R_v T \rho_l};\; K_{PP} = K_l + K_v \frac{p_v}{R_v T \rho_l}\; and\; K_{PT}$$
$$= K_v \frac{p_v}{R_v T^2}\left(L_v - \frac{p_c}{\rho_l}\right).$$

The coefficients C_{**} and K_{**} also depend on the temperature and capillary pressure. The values of these two variables are unknown at the beginning of timestep *j+1*. Their calculation is therefore based on the values obtained at timestep *j*, which is a specificity of the IMEX scheme.

Spatial discretisation implies calculating the value of some quantities between two points of the mesh. For this purpose, the mesh thicknesses are averaged and the coefficients K_{**} are calculated from a weighted average: $\Delta x_{i-1/2} = (\Delta x_i + \Delta x_{i-1})/2;\; \Delta x_{i+1/2} = (\Delta x_i + \Delta x_{i+1})/2;$ $K_{**i-1/2} = (K_{**i} * \Delta x_i + K_{**i-1} * \Delta x_{i-1})/(\Delta x_i + \Delta x_{i-1})$ *and* $K_{**i+1/2} = (K_{**i} * \Delta x_i + K_{**i+1} * \Delta x_{i+1})/(\Delta x_i + \Delta x_{i+1})$.

The same discretisation method and the same driving potentials are used to define the boundary conditions and the following equations are obtained:

$$j_{sext}^{j+1} = h_{conv,m}\left(p_{v,\,ext}^{j+1} - p_{v,\,sext}^{j}\left(1 + \frac{1}{\rho_l R_v T_{sext}^{j}}\left(p_{c,sext}^{j+1} - p_{c,sext}^{j}\right)\right)\right) + j_{rain,abs} \quad (9)$$

$$j_{sint}^{j+1} = h_{conv,m}\left(p_{v,\,int}^{j+1} - p_{v,\,sint}^{j}\left(1 + \frac{1}{\rho_l R_v T_{sint}^{j}}\left(p_{c,sint}^{j+1} - p_{c,sint}^{j}\right)\right)\right) \quad (10)$$

$$q_{sext}^{j+1} = h_{conv,th}\left(T_{ext}^{j+1} - T_{sext}^{j+1}\right) + L_v h_{conv,m}\left(p_{v,\,ext}^{j+1} - p_{v,\,sext}^{j}\left(1 + \frac{1}{\rho_l R_v T_{sext}^{j}}\left(p_{c,sext}^{j+1} - p_{c,sext}^{j}\right)\right)\right) + j_{rain,abs} c_l\left(T_{ext}^{j+1} - T_{ref}\right) + \alpha q_{SW,inc} + q_{LW} \quad (11)$$

$$q_{sint}^{j+1} = h_{conv,th}\left(T_{int}^{j+1} - T_{sint}^{j+1}\right) + L_v h_{conv,m}\left(p_{v,\,int}^{j+1} - p_{v,\,sint}^{j}\left(1 + \frac{1}{\rho_l R_v T_{sint}^{j}}\left(p_{c,sint}^{j+1} - p_{c,sint}^{j}\right)\right)\right) + q_{LW} \quad (12)$$

The variables at the surfaces are approximated by their value at the nearest node.

2.3. Validation by inter-model comparison

The objective of this part is to check that the updated method provides satisfactory results. This validation is performed by comparison with a reference tool, Delphin 6.1.2 (Fechner et al., 2020), which has been widely used and validated (Sontag et al., 2013). Delphin is a simulation programme developed for calculating the coupled transfers of heat, humidity, air, pollutants and salt in 1D, 2D or 3D. In our study, it was only used to describe the moisture and heat transfer through a multi-layer wall in 1D. The validation methodology is explained in detail in Ruiz et al. (2023) and only a brief description is given here. It consists of assessing the gap between results simulated with our method and those obtained using Delphin. Six variables are studied: temperature and vapour pressure at the interior surface, temperature and vapour pressure at the exterior surface, average temperature in the wall, and water content integrated over the whole wall. For each variable, threshold values for the error between our method and Delphin were set to: an absolute error of 1°C for temperature, and a relative error of 5% for vapour pressure and of 10% for water content. The times when these thresholds were exceeded were calculated. If the duration when the threshold value was exceeded was less than ten percent of the simulation time, the results were assumed to be satisfactory. Many cases were tested, including fifteen wall compositions (Appendix A – Table A1) and three climates (the temperate climate of Cahors in France, the hot and dry climate of Aswan in Egypt, and the hot and humid climate of Manaus in Brazil). All these study cases were simulated over a period of one year. The boundary conditions were always calculated considering the urban form of Cahors.

Results obtained with this modified version were always satisfactory for all the cases studied (Appendix A – Fig. A1) with the mesh version presented in Section 2.2. This means that the new assumptions and modifications made are appropriate.

3. Integration of moisture transfer through walls into TEB

The numerical method for solving hydrothermal transfer at the urban scale has been presented and validated in the previous section. The steps involved in integrating this method into TEB are detailed in this section, including the necessary adaptations regarding material properties, meshes, boundary conditions and the solving of the transfers in the walls.

3.1. TEB brief description

TEB is an urban climate model, which has been developed to simulate thermal, radiative, hydric and turbulent exchanges between the city and the atmosphere (Masson, 2000). The simulations can be performed from the neighbourhood scale to the city scale. An urban zone is represented by a grid with many points, representing each neighbourhood. The 3D geometry of the city in each grid mesh is simplified by an average 2D urban canyon, which means that buildings are not simulated individually. The TEB model incorporates the BEM (Building Energy Model) module, which simulates the energy behaviour of buildings (Bueno et al., 2012). Buildings are represented by a single thermal zone and the thermal inertia of the interior materials is modelled by a generic thermal mass (**Fig. 3**). This module can simulate building occupancy, internal gains, HVAC (Heating, Ventilation and Air-Conditioning) equipment, infiltration through the building envelope, windows and associated shading devices. TEB thus assesses the building energy consumption and quantifies the interactions between the buildings and the canyon microclimate.

The conditions in the urban canyon are calculated by considering many phenomena, such as the interaction with buildings, the releases from traffic or industry, the effect of gardens and different types of vegetation, the exchanges with the ground and the atmosphere, and radiative trapping and shadows. The comfort of pedestrians in the urban canyon is assessed using the UTCI (Universal Thermal Climate Index) (Bröde et al., 2010; Jendritzky et al., 2008). The calculation of this outdoor comfort index is integrated in TEB. It uses the main climatic variables affecting comfort (temperature, humidity, radiation and wind) and a physiological model.

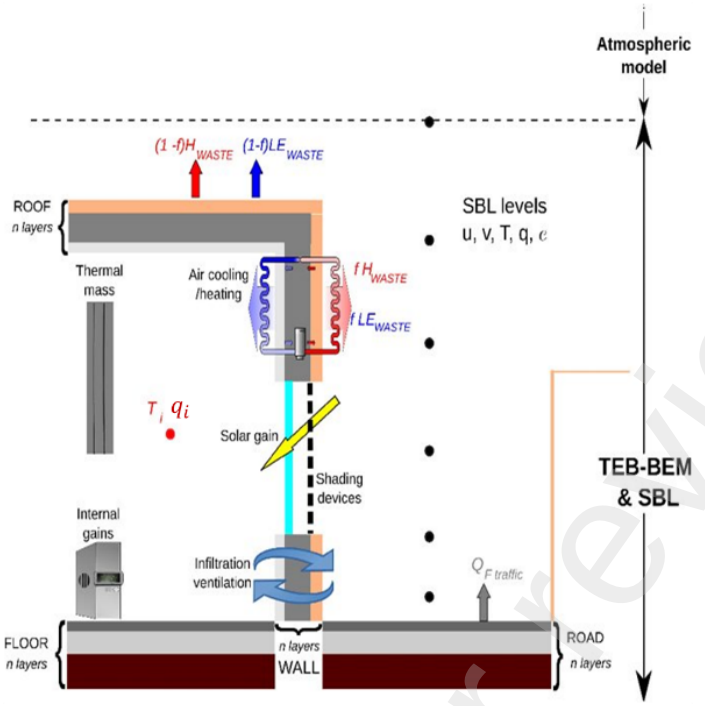

Fig. 3. Description of BEM (taken from Bueno et al. (2012).)

Concerning the consideration of moisture, TEB performs a mass balance to calculate the specific humidity in the urban canyon by considering anthropogenic moisture emissions (due to buildings and traffic), and moisture exchanges with the atmosphere, vegetation, road and soil. The BEM module can calculate the specific humidity of the indoor air, from a mass balance taking internal moisture gains, and vapour transfers due to window opening, air infiltration or HVAC equipment, into account. The TEB model thus already allows for complete indoor and outdoor mass balances, since it considers the main moisture phenomena at the urban scale. However, it currently neglects moisture transfers through the walls. Similarly, rainfall interception, evaporation and runoff are currently taken into account at roof and ground level, but not yet at wall level.

3.2. Simulation of wall hygrothermal behaviour

The current version of TEB solves heat transfer in 1D through walls (**Fig. 4**). It considers only heat transfer by conduction in a material assumed to be dry; all other hygrothermal phenomena are neglected. The heat equation used to describe walls is the following:

$$C_{mat}\frac{\partial T}{\partial t} = \frac{\partial}{\partial x}\left(\lambda \frac{\partial T}{\partial x}\right) \quad (13)$$

where C_{mat} is the volumetric heat capacity of the material $(J.m^{-3}.K^{-1})$

TEB considers spatial variations of thermal properties according to material layers but it neglects the temporal evolution of thermal properties according to the amount of moisture in each layer.

The integration of coupled mass and heat transfer involves implementing a second equation to solve the mass balance and also completing the heat equation by adding the hydric processes. This corresponds to equations (2) and (1), respectively, as the heat storage in the liquid phase, the evolution of the thermal conductivity as a function of the water content, and the heat transfer with the vapour phase must be added. These phenomena are integrated by applying the method presented in Section 2.

The addition of moisture transfers makes it possible to consider latent exchanges between the wall and the indoor and outdoor environments, as well as the effects of rain (**Fig. 4**). This new version of TEB can be used to quantify the impact of new phenomena, such as the evaporative cooling potential at the wall surface, the moisture buffering capacity of the materials and the effect of water contained in the pores on the thermal conduction of the walls.

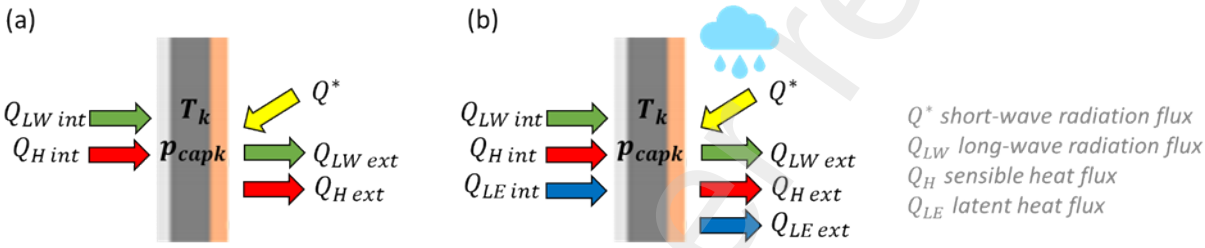

Fig. 4. Wall simulation in TEB (a) before and (b) after integration of hydric transfer.

However, the addition of moisture transfers is not limited to the modification of the equations describing the wall. It is also necessary to adapt the input data concerning the characteristics of the materials and the definition of the boundary conditions.

3.3. New input data

The walls simulated in TEB are multi-layer walls, i.e. they are composed of several materials. So far, the input data for defining the materials has been restricted to the thickness of the material layer, the dry thermal conductivity and the volumetric heat capacity.

The new version of TEB considers the evolution of thermal conductivity according to water content. The following equation is used to calculate the wet thermal conductivity (Nicolai, 2007):

$$\lambda = \lambda_{\mathrm{dry}} + \lambda_{\mathrm{w}}.\mathrm{w} \qquad (14)$$

with λ_{dry} the dry thermal conductivity of the material ($Wm^{-1}K^{-1}$) and λ_w the thermal conductivity of liquid water ($Wm^{-1}K^{-1}$).

To describe the hydric behaviour of materials, it is essential to add parameters that provide the model with information on the moisture storage capacity, the liquid water conductivity and the water vapour diffusion. These three characteristics change with the humidity in the wall. Their evolution according

to moisture in the layer can be described in three different ways: fixed as a constant, defined by a list of points, or using a model. The method is chosen depending on data availability and material characteristics.

The model integrated in TEB to describe the moisture retention curve is based on the work of Durner (1994). Thus, the water content is computed from capillary pressure using a multimodal expression:

$$w(p_c) = w_{sat} \sum_{i=1}^{N} l_i \left[1 + \alpha_i |p_c|^{n_i}\right]^{-m_i} \tag{15}$$

with $\sum l_i = 1$ and $m_i = 1 - \frac{1}{n_i}$

The liquid conductivity is calculated using the Mualem model, which was originally designed to calculate the hydraulic conductivity of soil (Mualem, 1976; Priesack and Durner, 2006) :

$$K_l = K_{l,sat} s^{\tau} \left[\frac{\sum_i l_i \alpha_i \left(1 - \left(1 - s_i^{1/m_i}\right)^{m_i}\right)}{\sum_i l_i \alpha_i} \right]^2 \tag{16}$$

with $K_{l,sat}$ the liquid conductivity at saturation (s), $s = \frac{w}{w_{sat}}$ and $s_i = \frac{w_i}{w_{sat}} = l_i \left[1 + (\alpha_i |p_c|)^{n_i}\right]^{-m_i}$

Note that the TEB user has the choice of providing the coefficients necessary to calculate these two models or of directly providing a list of points linking the variable to be calculated and the capillary pressure or the water content. In the second case, the values of the quantities are then calculated by interpolation.

Then, the vapour transfer through walls is calculated using the water vapour permeability. The following expression links this coefficient with the water vapour resistance factor:

$$K_v = \frac{D_{v,air}}{\mu R_v T} \tag{17}$$

with μ the water vapour resistance factor (-) and $D_{v,air}$ the diffusion coefficient of water vapour in air $(m^2.s^{-1})$.

So, the water vapour permeability coefficient can be defined by entering a function or a list of points, but there is a third option. In fact, Künzel (1995) suggests considering the vapour transfer coefficient to be constant, as it is almost constant in the sorption region and vapour transfers mainly take place in this region.

3.4. Dynamic calculation of boundary conditions

The boundary conditions are calculated dynamically during the run time, taking the impact of the wall on its environment into account. The TEB model calculates the hygrothermal conditions in the urban canyon and inside the buildings at each timestep and these data are then used to calculate the boundary conditions of the wall at the next timestep.

In the TEB model, only one thermal building zone is simulated, which means that the walls are not discretised according to floors. Average boundary conditions are therefore determined for the entire façade, using the mean temperature, the mean wind speed and the mean specific humidity in the urban canyon.

3.4.1. Thermal and radiative boundary conditions

The version of TEB before the integration of moisture transfers considers the thermal and radiative boundary conditions in a very comprehensive way. At the inner surface, the following exchanges are taken into account:

- Long-wave radiation exchanges between the wall surface studied and other interior surfaces (mass, floor, other walls and windows),
- Internal radiative gains,
- Load from solar heat gain,
- Thermal convection between the wall surface and the indoor air.

At the exterior wall surface, the boundary conditions are calculated from:

- Thermal convection between the façade and the outside air,
- Solar radiation,
- Long-wave radiation exchange between the façade under study and the other façades, the ground, snow, the atmosphere, and also with the windows of other buildings.

3.4.2. Hydric boundary conditions

The integration of the moisture transfers through the walls implies adding boundary conditions reflecting the moisture exchanges between the wall and its environment. The two phenomena to be added are mass convection and driving rain.

3.4.2.1. Mass convection

Mass convection takes place at both the inner and outer surfaces of the wall. It reflects the exchange of moisture between the wall and its environment. It involves both a mass boundary condition and a thermal boundary condition, which is due to the latent heat of water vapour:

$$j_{conv,m} = h_{conv,m}\left[p_{v,env} - p_{v,sat}(T_{surf})exp\left(\frac{p_{c,surf}}{\rho_l R_v T_{surf}}\right)\right] \quad (18)$$

$$q_{conv,m} = L_V.h_{conv,m}\left[p_{v,env} - p_{v,sat}(T_{surf})exp\left(\frac{p_{c,surf}}{\rho_l R_v T_{surf}}\right)\right] \quad (19)$$

The TEB model calculates the thermal convection coefficients at the inner surface by applying the DOE-2 model (Lawrence Berkeley Laboratory (LBL), 1994) and, at the outer surface, using the model of Rowley et al. (1930, 1932). Then, the mass convection coefficient is easily calculated by applying the Lewis relation (Janssen et al., 2007):

$$h_{conv,m} = 7.7 * 10^{-9} \; h_{conv,th} \quad (20)$$

Mass convection also involves the vapour pressure difference between the surface and the ambient air. The vapour pressure of the ambient air is derived from the specific humidity calculated from the indoor or outdoor mass balance.

3.4.2.2. Wind-Driven Rain

The other boundary condition to be integrated is the rain absorbed by the wall. The TEB tool allows the local wind speed to be estimated inside the canyon. TEB simulates a one-dimensional wind profile within the urban canyon by using a drag force approach and considering the effect of vegetation and urban canopies (Hamdi and Masson, 2008; Masson and Seity, 2009). The local wind speed is an important criterion for estimating the Wind-Driven Rain (WDR). The method chosen to integrate this phenomenon is based on the work of Straube and Burnett (2000), as their formula integrates the local wind speed. The following formula is used to calculate the driving rain incident on the façade:

$$j_{rain,inc} = \frac{1}{V_t}.RAF.u(z).j_{rain}.\cos(\theta) \quad (21)$$

with V_t the raindrop terminal velocity of fall, RAF the Rain Admittance Factor, *u(z)* the local wind speed at the height of the studied point z, j_{rain} the amount of precipitation ($kg.m^{-2}.s^{-1}$), and θ the angle between the wind direction and the line normal to the wall.

For the calculation of the falling velocity of a raindrop as a function of its diameter, the equation of Dingle and Lee (1972) is used:

$$V_t(d) = -0.166033 + 4.91844\,d - 0.888016\,d^2 + 0.054888\,d^3 \quad (22)$$

with d the raindrop diameter.

The terminal velocity of an average raindrop is estimated from the mean raindrop diameter. Blocken and Carmeliet (2010) suggest the following formula to calculate the mean raindrop diameter, according to the work of Best (1950):

$$\overline{d} = 1.105 r^{0.232} \quad (23)$$

The incident rain flux used by TEB represents an average flux incident on the wall. The wind speed used in the equation is therefore not the wind speed at a specific height, but the mean wind speed simulated within the canyon. Concerning the local wind direction, TEB does not allow a wind direction to be simulated inside the urban canyon, so it is assumed to be equal to the direction above the canyon. However, the local wind speed generally used in Straube and Burnett's equation (Straube and Burnett, 2000), corresponds to the wind speed in a free wind region and thus outside the region disturbed by the buildings.

The RAF coefficient allows calculations to pass from the WDR intensity in free field to the rain deposition on the façade of the building (Straube, 2010). This coefficient depends not only on local aerodynamics but also on raindrop diameter, building shape and wind angle of attack. In our case, the local wind speed already took the local aerodynamics into account, but the other factors still needed to be considered by a coefficient. The choice of the value for the RAF coefficient is complex and Straube and Burnett (2000) suggest values for this coefficient for only a few configurations.

The use of a semi-empirical method for the prediction of WDR implies a high level of uncertainty (Zhou et al., 2023). Nevertheless, the prediction of WDR in an urban climate model like TEB cannot be achieved by CFD methods for each neighbourhood geometry studied. It was therefore necessary to update these semi-empirical relations and to suggest suitable coefficients to work with the local wind speed in the urban canyon.

However, not all the incident flux can be systematically absorbed by the wall. The maximal absorbed rain flux is calculated according to the moisture conditions in the wall, from the following equation:

$$j_{rain,max} = -\left(K_l(w_{sat}), K_l(w^{elem})\right).\frac{p_c^{elem}}{x^{elem}} \quad (24)$$

with $j_{wdr,max}$ the maximum water flow into the boundary element *($kg.m^{-2}.s^{-1}$)*, w_{sat} the saturation water content of the material *($kg.m^{-3}$)*, w^{elem} the current water content in the boundary element *(kg.*

m^{-3}), p_c^{elem} the capillary pressure in the boundary element *(Pa)* and x^{elem} the thickness of boundary element *(m)*.

The absorbed rain flux corresponds to the minimum value between the incident rain flux at the façade and the maximum flux:

$$j_{rain,abs} = \min(j_{rain,inc}, j_{rain,max}) \quad (25)$$

Moreover, heat flux is associated with the mass flux of absorbed rain:

$$q_{rain} = c_l(T_{can} - T_{surf}).\, j_{rain,abs} \quad (26)$$

This equation expresses the transition of rainwater temperature from the canyon temperature to the wall surface temperature.

In addition, the interception of rain by the wall has an impact on the distribution of the rainfall on the scale of the urban canyon (see Appendix B).

3.4.3. Management of timestep reduction

As explained in section 2.2, the method developed for solving coupled transfers generally works with a timestep of five minutes, but involves adding sub-timesteps of ten seconds, at moments critical for numerical stability. The urban model TEB generally uses a fixed timestep of five minutes. Its numerical stability does not require a reduction of the timestep. Therefore, this adjustment mechanism was only applied to the transfers in the walls (as necessary for stability), but not to the whole TEB model. Thus, when a critical moment was identified, the timestep for hygrothermal transfers through walls was reduced while the timestep for the other physical processes involved in the urban climate model remained fixed at five minutes. This method enabled a reasonable calculation time to be kept for the whole model. Concerning the calculation of the boundary conditions of the walls, indoor and outdoor conditions are calculated every five minutes, including in the case of a decrease of the timestep. Thus, when the timestep is decreased, we consider that the elements needed for computation of boundary conditions (temperature and humidity of the environment, radiative fluxes and driving rain) remain the same for all the sub-timesteps of ten seconds and those until the end of the five minute timestep.

4. Hygrothermal simulation of the historical district of Cahors

In this section, the new version of TEB is tested in a case study of the medieval centre of Cahors. The model had to be configured to be representative of this neighbourhood. The hygrothermal conditions inside the simulated building are compared to those recorded in a building of Cahors and the results

obtained before and after the integration of moisture transfers are also compared. The impact of hydric transfers through the walls is thus discussed.

4.1. Description of the case studied

This study focused on the medieval city centre of Cahors (Fig. 5), a small town in the South of France (44°26′54″N 1°26′29″E). It is characterized by a dense, complex urban form with very narrow streets having two main orientations: North-South and East-West (Claude, 2018).

Buildings date mainly from the 13th century (Malagoni de Almeida, 2022). Since that time, they have undergone successive renovations, resulting in a high degree of heterogeneity of the walls. Two main typologies of walls can be found in the medieval district of Cahors: walls made of massive brick and wood-frame walls filled with bricks (Claude, 2018; Claude et al., 2019). The historical walls of this district are subject to heritage preservation constraints. Therefore, when they are retrofitted, their outside appearance must be preserved. In the scope of the ENERPAT project, the retrofitting of these walls using bio-based materials was studied, considering the heritage conservation constraint and also the durability of the wall (in particular the growth of mould) (Claude et al., 2019). As part of this work, walls were renovated using a hemp-lime interior insulation and instrumented (Claude et al., 2017). A weather station was also set up on a roof in the medieval centre, close to the instrumented building, in order to record local weather data (**Fig. 5**).

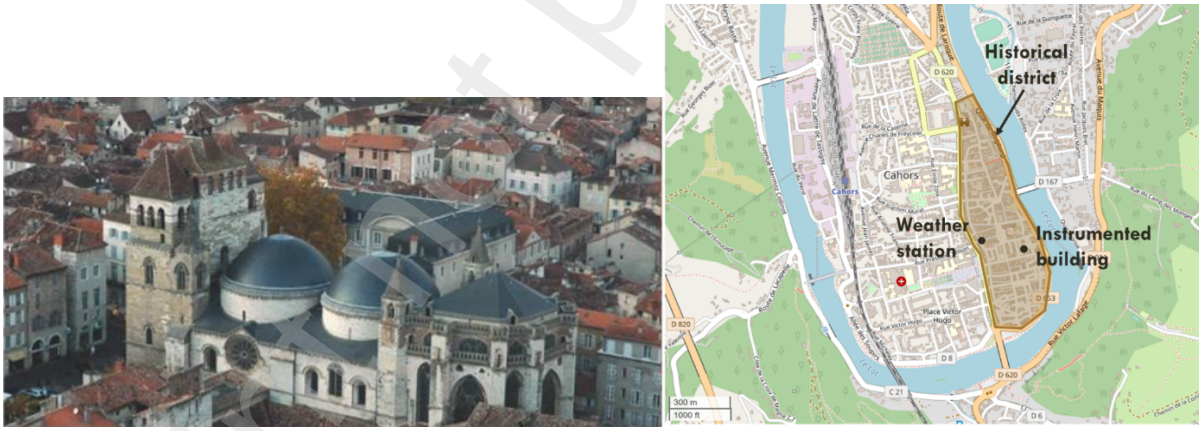

Fig. 5. Medieval district of Cahors (taken from Charrier (2013)) and location of the instrumented area.

Data measured in a monitored building were used to validate the modified version of TEB, including moisture transfer through walls. The building studied had massive walls (40 cm thickness of bricks). Not all walls of the building had been retrofitted with the same techniques. Most of them had been insulated from the inside with polystyrene, while the first-floor façade facing west had been retrofitted with 15 cm of hemp and lime insulation. This wall was the only instrumented wall in the building and was therefore used for model validation (**Fig. 6**). The hypothesis made for the TEB configuration was therefore that the wall composed of 40 cm thickness of bricks and insulated with 15 cm of hemp-lime, was representative of the district. It is

important to underline that, in reality, this wall was not totally representative of the medieval centre. However, the objective of this work was to validate the model and not to study the behaviour of the medieval centre of Cahors.

Fig. 6. View of the west facade of the building studied.

4.2. In-situ instrumentation

The instruments installed in the building recorded not only measurements of indoor conditions but also those in the wall (**Fig. 7**). Thus, temperature and relative humidity were recorded with a thermohygrometer (KIMO KH50) in the room adjacent to the wall under study. The surface temperature was measured on the indoor surface of the wall, using type K thermocouples. Sensors (Honeywell HIH 4602-C) detected the hygrothermal conditions in the middle of the insulation and at the interface between the insulation and the brick.

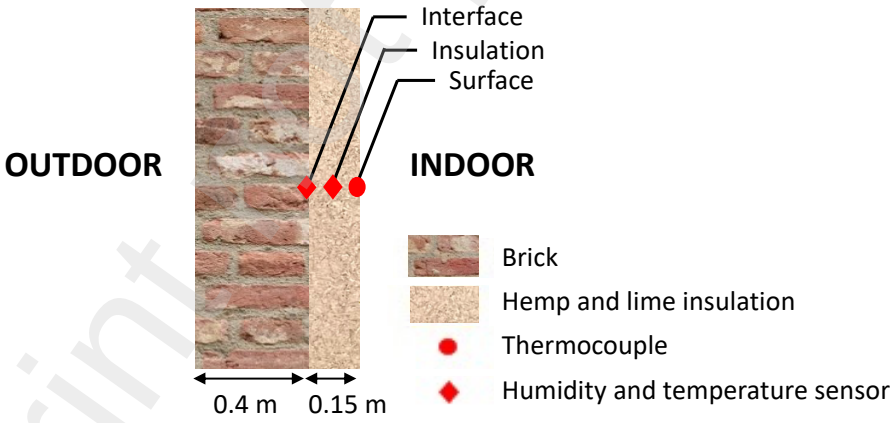

Fig. 7. Description of the instrumented wall.

A weather station (Vantage Pro 2 Plus) was also installed to measure local outdoor conditions. It was positioned on a roof in the medieval centre of Cahors (**Fig. 8**) to provide data on temperature, relative humidity, amount of precipitation, solar radiation, and wind speed and direction.

Fig. 8. Weather station located on a roof in the medieval centre of Cahors.

4.3. Configuration of the simulation

The objective of this part was to provide input parameters to TEB, which described the study case. The urban form of the district is very dense and contiguous; the indicators provided by Claude (2018) were used. The RAF coefficient, used for the calculation of the WDR, was set to 0.2 to match the in-situ measurement of relative humidity inside the studied wall. As TEB allows the simulation of various street orientations, the two main street orientations were simulated (**Fig. 9**). The instrumented wall is the wall B.

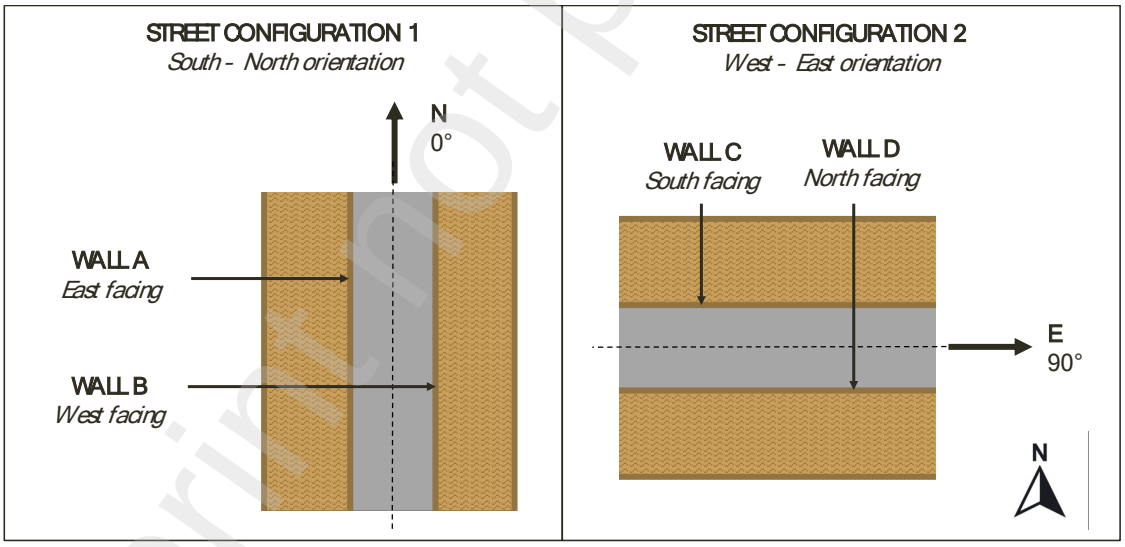

Fig. 9. Description of the two street configurations simulated (view from above.)

The buildings were assumed to have undergone a first renovation with modern materials, i.e. roof insulation with mineral wool, installation of double glazing in the windows, insulation of the walls with hemp-lime and reduction of the air permeability. The medieval town centre is facing a loss of inhabitants to more modern dwellings, mainly due to the lack of comfort and to fuel poverty. The buildings were therefore considered unoccupied, no ventilation or air conditioning equipment was running, internal

loads were set to zero and wood shutters were always closed. The heating worked only during cold periods, with a set point of 19 °C. **Table 2** summarises the input data used to describe the medieval town centre of Cahors.

Table 2
Properties of the average street simulated in TEB.

Property	Value	Unit
Vertical-to-horizontal building area ratio	1.8	
Building height	12	m
Building density	0.589	
Roughness length	1.5	m
Internal gains	0	W/m²
Glazing-to-wall ratio	0.1	
Window construction	Double-glazing	
U-value window	2	W/(m²/K)
Shading devices	Permanent	
Solar transmittance of shade	0	
Infiltration	4	Vol/h at 50 Pa
Mechanical ventilation	None	
Heating system	Variable (**Fig. 10**)	
Air conditioning system	None	

Table 3 summarises the thermal and radiative properties of construction materials, used in roofs, walls, floors and masses for thermal inertia.

Table 3
Characteristics of the materials constituting the building.

Property	Material	Thickness (m)	Volumetric heat capacity ($J.m^{-3}.K^{-1}$)	Thermal conductivity ($W.m^{-1}.K^{-1}$)	Albedo	Emissivity
Roof						
Layer 1 (out)	Tile	0.02	1422900	1	0.25	0.8
Layer 2	Mineral wool	0.2	42500	0.04		
Layer 3 (in)	Plasterboard	0.02	765000	0.21		
Wall						
Layer 1	Brick	0.4	1292800	0.49	0.3	0.9
Layer 2	Hemp-lime	0.15	440000	0.107		
Floor						
Layer 1	Wood	0.2	800000	0.29		
Mass						
Layer 1	Wood	0.15	800000	0.29		

As explained in Section 3.3, further properties were needed to describe the hygrothermal behaviour of the walls in the modified version of TEB. The hygrothermal properties of the materials constituting the

walls were defined from the results of Claude's work (Claude, 2018), which includes a characterisation of the insulation based on hemp-lime and of 16th century bricks taken from the old centre of Cahors. The values used for thermal conductivity and volumetric specific heat are given in **Table 3**.

For hemp-lime, lists of points were used to describe the moisture retention curve and the evolution of the liquid conductivity as a function of the water content. For brick, both curves were described by applying the models associated with equations (15) and (17). For both materials, the vapour diffusivity coefficient was assumed to be constant. All the parameters used to describe the hydric behaviour of brick and hemp-lime are presented in detail in Appendix C.

4.4. Forcing data

The simulation time was divided into two phases: the initialisation phase and the comparison phase. The initialisation step lasted for one year, from 17th June 2020 to 17th June 2021. The purpose of this stage was to obtain suitable initial conditions in the wall at the beginning of the comparison phase. The comparison ran from 17th June 2021 to 1st January 2022 (more than six months) (**Fig. 10**).

The urban simulation of the TEB tool needs to be forced by a file of weather above the canyon. During the initialisation phase, data from the urban weather station were not available. Therefore, the weather forcing was computed using weather data from a station at a nearby aerodrome: the forcing data for temperature, specific humidity, horizontal rainfall, solar radiation, pressure, wind speed and direction were calculated using the measurements of Le Montat weather station, located about 10 km from the centre of Cahors. The only missing data was longwave radiation from the atmosphere, which was calculated from the formulas of Martin and Berdahl (1984) and Walton (1980). These equations required knowledge of the air temperature and the dew point temperature, which were obtained from the measurements at the station, and also of the cloud cover, which was not measured at this station. For the cloud cover, the value recorded by a weather station located at Gourdon (about 40 km from Cahors) was used.

During the comparison phase, the data from the weather station located on a roof in Cahors were available and could be used directly. This station provided almost all the variables necessary for the forcing (temperature, specific humidity, horizontal rainfall, solar radiation, pressure, wind speed and direction). However, the variables measured at this urban station did not allow the computation of long wave radiation from the atmosphere. The same method as in the initialisation phase was therefore applied.

The heating in TEB was programmed so as to be switched on during the same periods in the simulation as in the real building. It was thus activated from 17th June 2020 to 17th May 2021 and from 17th November 2021 to 1st January 2022. The fact that the heater was switched on did not mean that it ran continuously. It only heated when the indoor temperature was below the target temperature (19 °C).

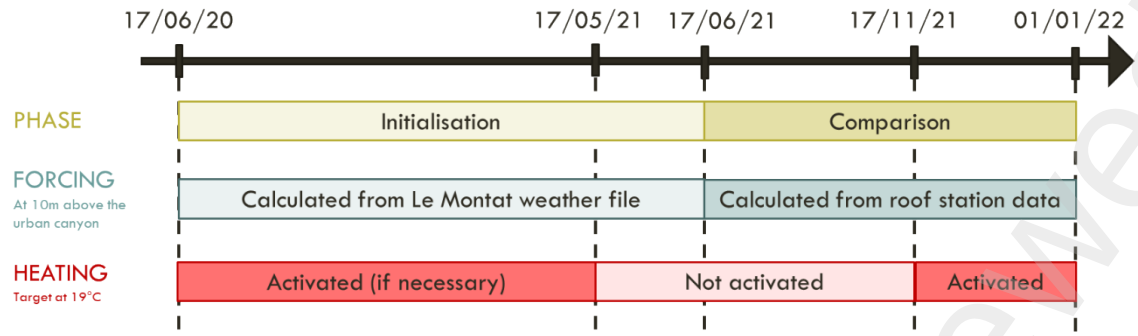

Fig. 10. Temporal representation of the different phases and the forcing data used.

Fig. 11 shows data recorded by the urban weather station and used for the TEB forcing data on conditions above the urban canyon during the comparison phase. Only the main variables are presented: temperature, relative humidity, horizontal solar radiation and the amount of precipitation on a horizontal plane.

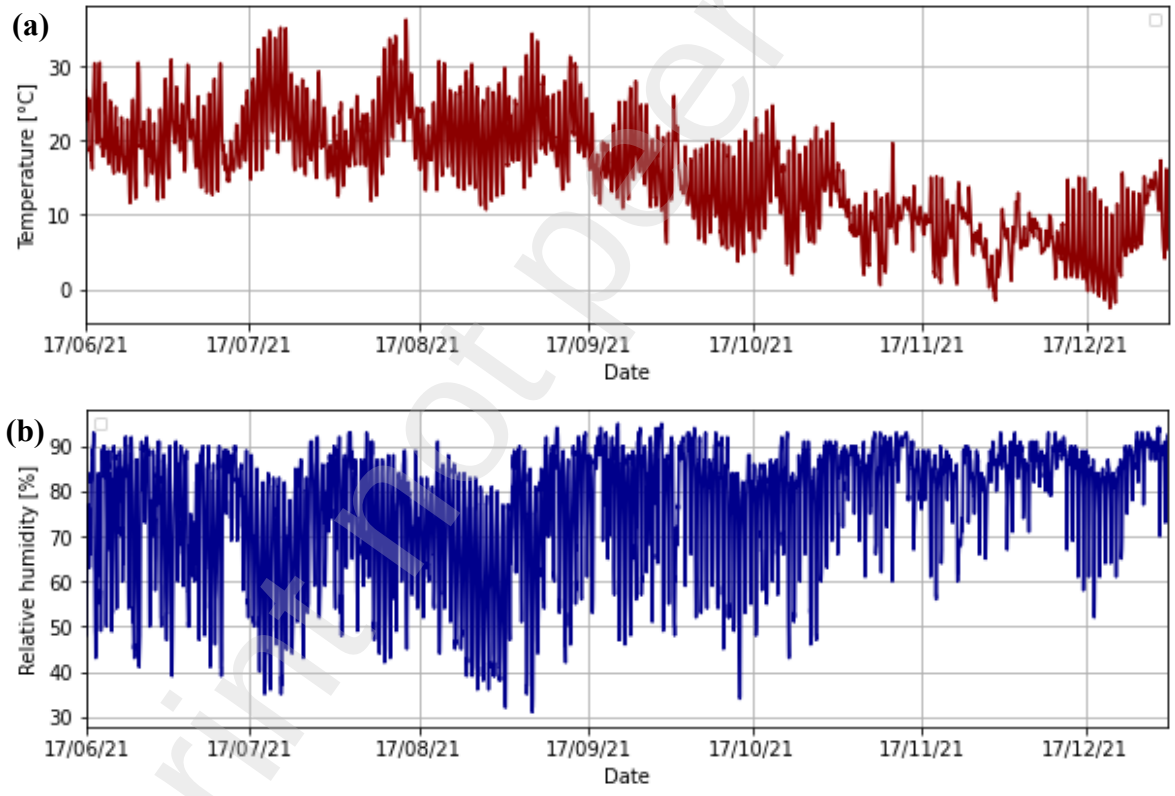

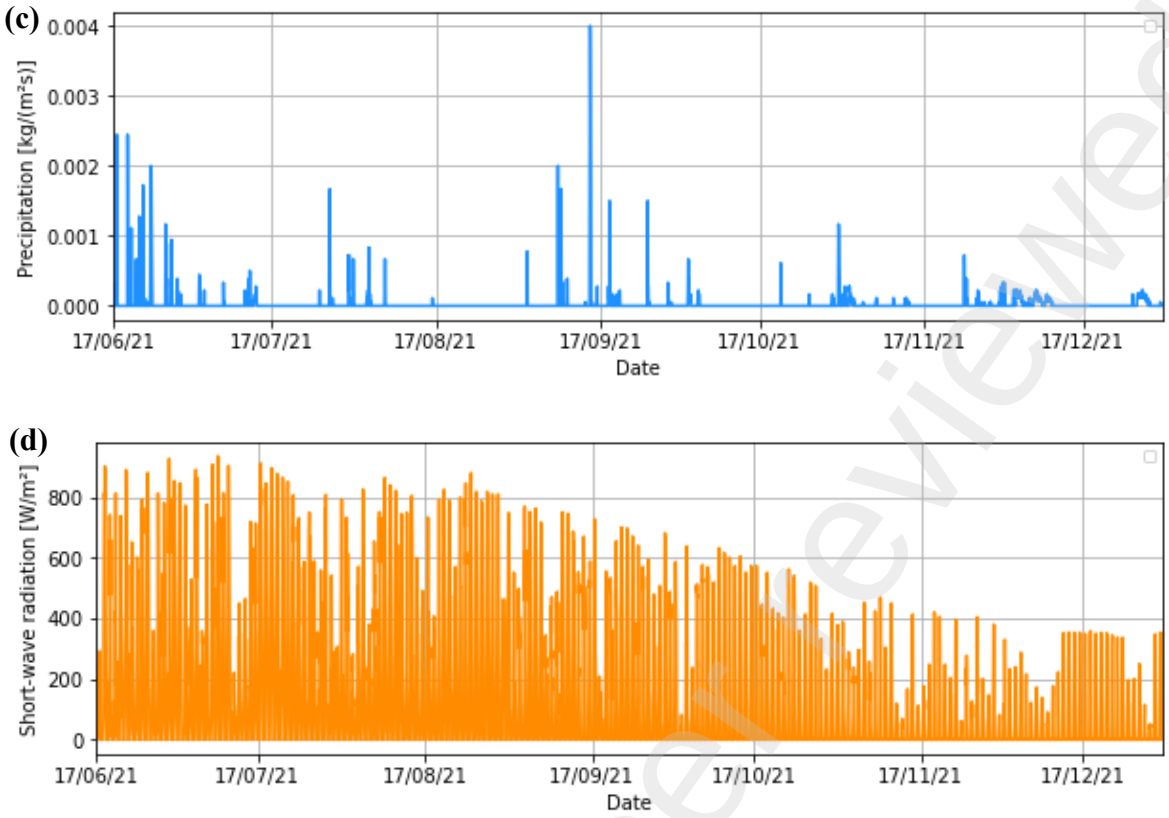

Fig. 11. Temperature (a), relative humidity (b), solar radiation (c) and precipitation (d) used for the forcing file of data above the urban canyon.

4.5. Assessment method

Calibration and validation of numerical models are key issues in order to obtain robust results when simulating historical buildings (Costa-Carrapiço et al., 2022a; Huerto-Cardenas et al., 2020; Panico et al., 2023). Several works have used in-situ data measured in old buildings to calibrate and/or validate their wall or building models (Andreotti et al., 2022; Hansen et al., 2018; Panico et al., 2023; Roberti et al., 2015; Şahin et al., 2015; Saïd et al., 1999). However, there is currently no consensus on the method to be used for comparing measured and simulated data (Costa-Carrapiço et al., 2022b). Huerto-Cardenas et al. (2020) suggest a reflection on this topic and provide guidelines for the parameters to be compared (in particular the importance of integrating a criterion on humidity) and the threshold values to be used for the validation. It is unrealistic to expect perfect agreement between simulated and measured data (Hens, 2015; Panico et al., 2023) as it is difficult for models to reflect real conditions The tools are based on more or less complete hypotheses concerning physical phenomena, geometry, wall composition, hygrothermal properties of materials, occupancy, and meteorological data. Uncertainties also exist on the representativeness of in-situ measurements (Akkurt et al., 2020; Costa-Carrapiço et al., 2022b).

To check the relevance of the model and of the assumptions made, the conditions simulated by TEB are compared with the measurements made in the instrumented building in Cahors (**Fig. 7**). The ability

of TEB to provide reliable simulations the study case was checked at four points: at the interface between brick and insulation, in the middle of the insulation, at the inner surface of the wall, and inside the building. Both temperature and relative humidity were verified at all these points, except at the surface, where only the temperature was recorded.

The gap between measured and simulated data was evaluated through two indicators: MAE (Mean Absolute Error) and Pearson coefficient, which measures the linear correlation between two sets of data.

$$MAE = \frac{\sum_{i=1}^{n} |m_i - s_i|}{n} \quad (27)$$

$$r = \frac{\sum_{i=1}^{n} (m_i - \overline{m}) \times (s_i - \overline{s})}{\sqrt{\sum_{i=1}^{n} (m_i - \overline{m})^2} \times \sqrt{\sum_{i=1}^{n} (s_i - \overline{s})^2}} \quad (28)$$

with m_i the measured value at time i, s_i the simulated value at time i, and n the number of timesteps.

Following Huerto-Cardenas et al. (2020), a first level of validation was considered when the MAE was lower than 1 °C or 5% RH. Another, less accurate, level of validation was defined by considering a threshold for MAE at 2 °C or 10% RH, which corresponded to the threshold for the second level of Huerto-Cardenas et al. (2020). At both validation levels, we estimated that the Pearson coefficient had to be greater than 0.7, to reflect a good correlation between measured and simulated values (**Table 4**). In cases where the values were outside these validation criteria, the simulation results were considered unsatisfactory. This method of validation was applied for the two variables and the four comparison points.

Table 4
Threshold values for the two validation levels.

	Level 1	**Level 2**
MAE (Mean Absolute Error)	≤ 1°C ≤ 5%RH	≤ 2°C ≤ 10%RH
r (Pearson coefficient)	> 0.7	> 0.7

4.6. Results

This section shows the results of the comparison between the measurements and the simulations using TEB. This will allow us to verify that the results simulated with TEB are satisfactory and thus to confirm the quality of the model and the relevance of the assumptions made concerning the definition of the neighbourhood, the building, and the materials.

Both versions of TEB (with and without moisture transfer through walls) are compared with in-situ measurements. The interest of integrated hygrothermal transfer is evaluated. The comparison of the two versions makes it possible to quantify the impact of the moisture transfers on the different points

studied: at the brick/insulation interface, in the middle of the insulation, on the inner surface of the wall, inside the building and also in the urban canyon.

4.6.1. Hygrothermal conditions in the wall

The first point of study corresponds to the interface between the brick and the insulation. Regarding temperature, the simulated data are close to the measurements made at the same point. Moreover, a similar trend is observed for both curves (**Fig. 12**). The MAE for temperature is approximately equal for both versions of TEB (**Table 5**). Thus, moisture transfer does not seem to have a great impact on the temperature at this point. The MAE for the modified version of TEB is 1.18°C. As the MAE is above 1°C, the validation is only level 2. Nevertheless, the results remain satisfactory, with a high Pearson coefficient of 0.992.

The relative humidity is validated at level 1 (the most accurate level). The model tends to overestimate the relative humidity in summer and underestimate it in winter. Nevertheless, the results remain satisfactory. The amount of moisture at the interface is strongly affected by WDR. The model and the coefficient used are therefore suitable to describe the driving rain incident on the first floor of this façade. On the other hand, it is not possible to compare the relative humidity between the two versions of TEB, since the version before integration does not calculate the humidity evolution inside the wall.

It should be remembered that TEB does not differentiate the floors in the calculation of the boundary conditions, which means that the entire wall, regardless of the floors, receives the same amount of rain and the same radiative flux. In addition, the mesh applied does not include any refinement at the interface between two layers of material. Taking these strong simplification assumptions into account, the results obtained are very satisfactory.

In the present study, the interface was the point that was most influenced by the definition of the exterior boundary conditions. The definition of the urban boundary conditions therefore seems relevant. In order to better verify the relevance of the urban boundary conditions, it would have been useful to position a sensor to measure the conditions inside the brick, closer to the external surface. However, the brick wall was too fragile to be drilled (drilling could have affected the stability of the wall).

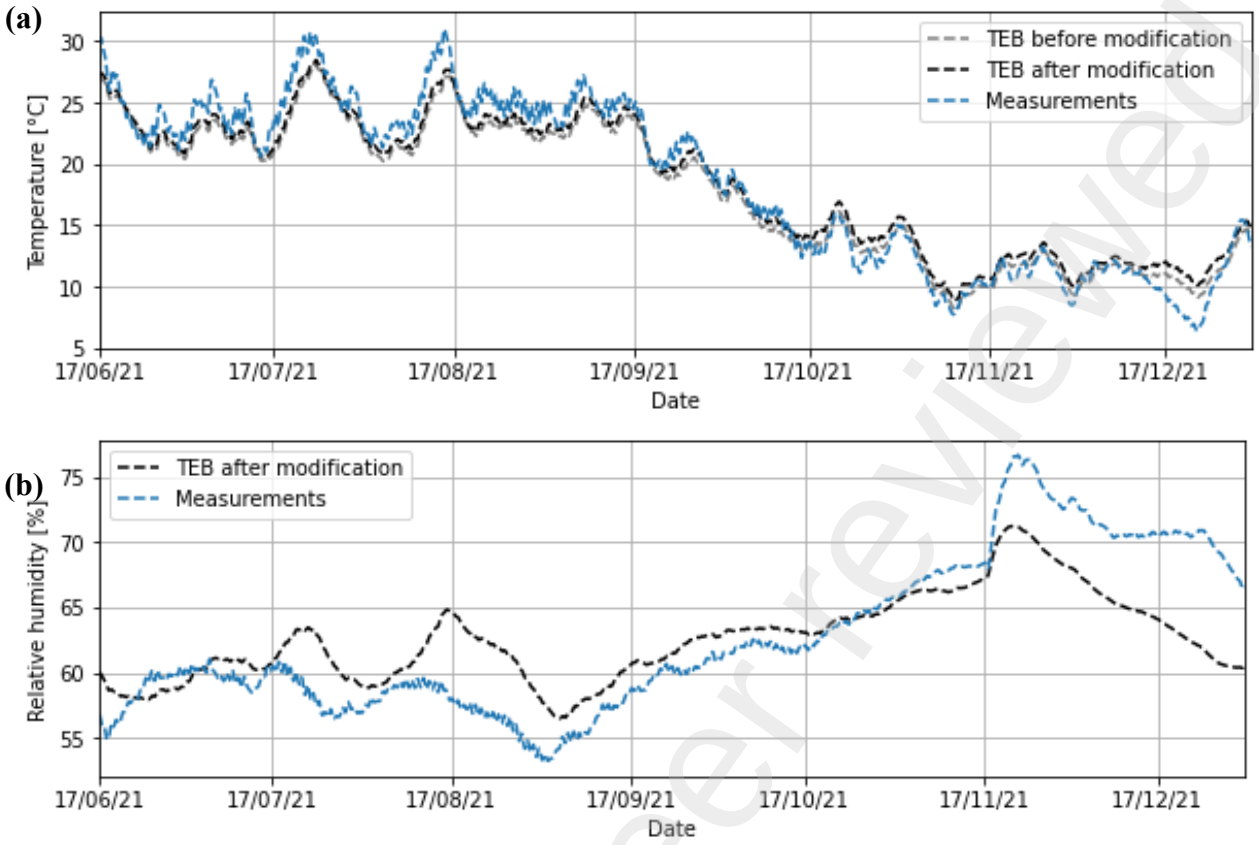

Fig. 12. Temporal evolution of simulated and measured temperature (a) and relative humidity (b) at the interface between brick and insulation from 17th June 2021 to 1st January 2022.

At the middle of the hemp and lime insulation, very good agreement is observed between measurements and simulated data for both temperature and relative humidity. Using the version of TEB that includes moisture transfer through walls, the validation is level 1, the most accurate level. In contrast, the results simulated by the unmodified version of TEB lead to a validation of level 2 as the MAE of temperature is slightly lower when moisture transfer is considered (**Table 5**). The hygrothermal properties used to describe the hemp-lime insulation are therefore appropriate.

At the level of the inner surface, only the temperature was measured and, so, studied. The simulation results are very close to the measurements: the calculated MAE is around 0.5°C and the Pearson coefficient of 0.99 shows a strong correlation (**Table 5**). This point of the wall is very strongly influenced by the indoor boundary conditions. The definition of the building therefore allows good simulation of the indoor conditions.

Table 5

Indicators on the error between the measured and simulated data at three points of the wall from 17th June 2021 to 1st January 2022 *(na = not applicable)*.

			Temperature	Relative humidity
INTERFACE	**MAE**	TEB before modification	1.24 °C	na
		TEB after modification	1.18 °C	2.92 %
	Pearson coefficient (r)	TEB before modification	0.992	na
		TEB after modification	0.992	0.823
	Validation level	TEB before modification	2	na
		TEB after modification	2	1
INSULATION	**MAE**	TEB before modification	1.07 °C	na
		TEB after modification	0.82 °C	1.22 %
	Pearson coefficient (r)	TEB before modification	0.989	na
		TEB after modification	0.987	0.923
	Validation level	TEB before modification	2	na
		TEB after modification	1	1
SURFACE	**MAE**	TEB before modification	0.41 °C	na
		TEB after modification	0.53 °C	na
	Pearson coefficient (r)	TEB before modification	0.992	na
		TEB after modification	0.989	na
	Validation level	TEB before modification	1	na
		TEB after modification	1	na

4.6.2.Indoor conditions

Regarding indoor temperature, good agreement is observed between simulated and measured data (**Fig. 13**). The MAE values are very satisfactory in both versions (**Table 6**). The difference between the simulated results from the two versions of TEB is very small, which shows that the moisture transfers have little impact on the indoor temperature in the configuration studied, i.e. an unoccupied building.

Previous works have shown a significant impact of the moisture buffer capacity on the indoor thermal conditions (Maalouf et al., 2014; Zhou et al., 2020). It would therefore be interesting to carry out a new study assuming that the building is occupied, to assess the impact of this situation in the context of the medieval centre of Cahors. Furthermore, considering the building as occupied would allow the comfort of the occupants and also the energy consumption to be evaluated.

In addition, a slightly larger discrepancy between the simulated and measured data was observed when the heating was switched on. This is because TEB simulates perfect control whereas, in real conditions, the indoor temperature fluctuates around the set temperature.

Concerning the relative humidity, a larger difference can be observed between the results of the two TEB versions (**Fig. 13**). The calculation of the indicators (MAE and Pearson coefficient) leads to a validation of level 1 for the version considering the moisture transfers through the walls and of level 2 for the version neglecting them. Moreover, not taking the moisture transfers through the walls into account leads to inconsistent values, with an indoor relative humidity exceeding 100%. Condensation should therefore occur, but TEB does not model condensation inside the building. Consideration of moisture transfer through the walls provides results that are closer to the values measured on site: the variations are smaller, and the peaks of relative humidity are reduced, which corresponds to the moisture buffering behaviour of hemp and lime insulation, a highly hygroscopic material.

In the simulation of this unoccupied building, the moisture balance inside the building is only impacted by the air infiltration through the building envelope and the exchanges through the walls. In reality, other phenomena are involved, such as moisture exchanges with other internal materials (internal walls, floor, etc.), and also transfer at the level of the roof and the ground, or capillary rise from the ground to the walls. However, these phenomena are currently neglected in TEB. Therefore, if the accuracy of the indoor relative humidity prediction is to be increased, these phenomena should be integrated into TEB. For this study, the level of accuracy obtained is considered satisfactory.

It is also relevant to note that the measurements were made in a given room, on the first floor and adjacent to the west-facing façade, whereas TEB does not simulate the conditions room by room but considers the building as a single thermal zone. Finally, the new version of TEB gives satisfactory results and thus correctly represents the hygrothermal behaviour of the old building. It will therefore be a good tool for the simulation of the old town centre of Cahors on an urban scale and can thus be used to evaluate different retrofit scenarios.

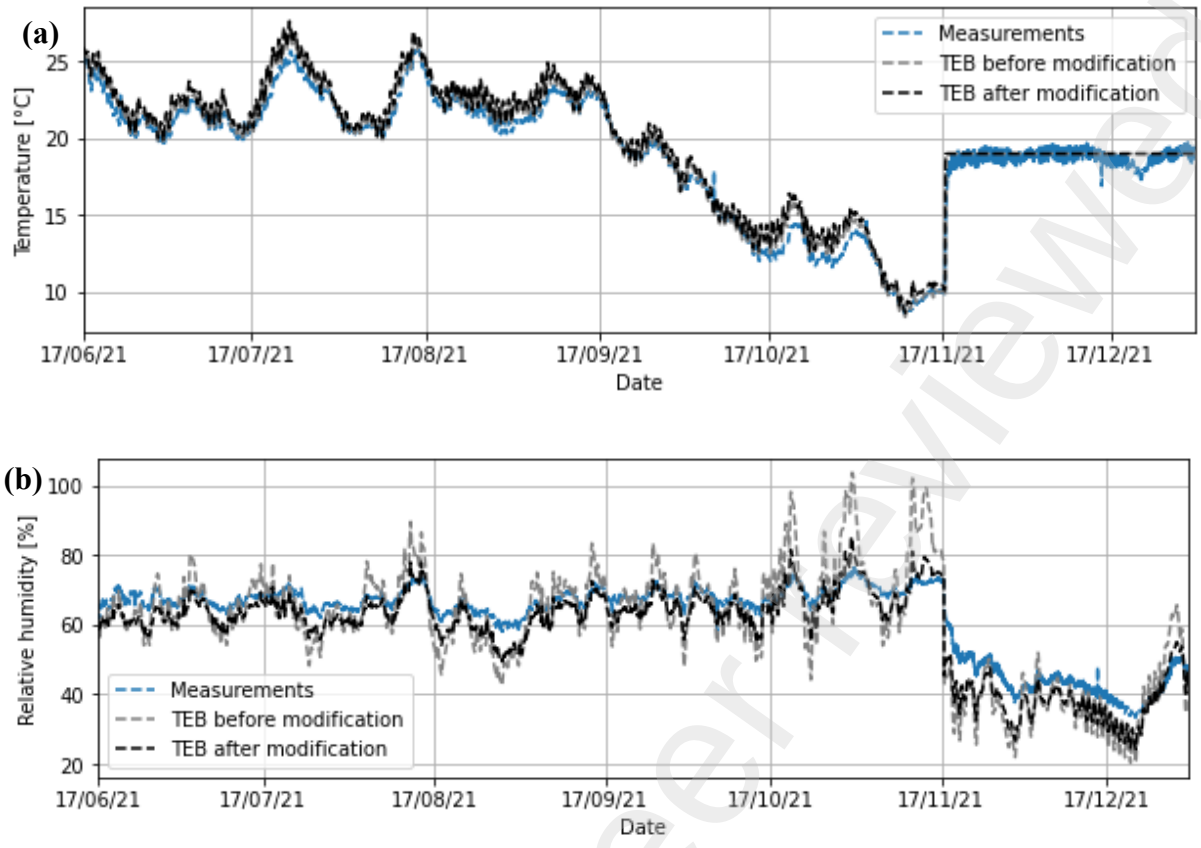

Fig. 13. Temporal evolution of simulated and measured temperature (a) and relative humidity (b) in the room studied from 17 th June 2021 to 1st January 2022.

Table 6
Indicators of the error between the measured and simulated data in the room studied from 17th June 2021 to 1st January 2022.

		Temperature	**Relative humidity**
MAE	TEB before modification	0.54 °C	6.74 %
	TEB after modification	0.73 °C	4.43 %
Pearson coefficient (r)	TEB before modification	0.992	0.878
	TEB after modification	0.990	0.967
Validation level	TEB before modification	1	2
	TEB after modification	1	1

4.6.3.Impact on urban canyon conditions

The objective of this section is to quantify the impact on the urban canyon conditions of considering moisture transfer through walls. Saneinejad et al. (2014, 2012) have shown that drying the façade after a rainy event can lead to a reduction of canyon temperature and UTCI by evaporative cooling and thus improve pedestrian comfort. However, this experiment was performed in simplified weather conditions, since the windward wall suddenly became capillary saturated.

This section investigates the potential of evaporative cooling, using the second street configuration and the south-facing wall C (**Fig. 9**) from 23rd to 26th June 2021. This case was chosen because it corresponds to one of the highest absorbed rain fluxes during the summer of 2021. This study allowed the phenomenon to be evaluated in real conditions when the wall surface did not reach water saturation and in the specific context of a very narrow street.

The rain event took place during the night of 23rd to 24th June 2021. Thus, wall C absorbed rainfall and the water content at the surface increased (**Fig. 14** a and b). The relative humidity was almost 100% until 9:30 a.m. and then decreased, matching the drying of the façade (**Fig. 14** c).

The comparison of the two versions of TEB evaluates the impact of the moisture exchanges on the conditions in the canyon. A decrease in the surface temperature of wall C of up to about 2 °C is observed during the wetting and drying phases (**Fig. 14** d). Thus, the version of TEB that considers moisture transfer through the walls simulates lower heat and radiative fluxes from the façade to the canyon. **Fig. 14** (e and f) shows a decrease of up to 24 W/m² for the sensible flux and up to 7.5 W/m² for the long-wave radiative flux.

Nevertheless, the decrease in the surface temperature of wall C and in the fluxes from the wall to the canyon is not sufficient to significantly impact the temperature and, more generally, the comfort in the canyon. The difference between the two TEB versions does not exceed 0.05 °C for the canyon temperature and 0.1 °C for the UTCI.

Finally, the potential for cooling by evaporation seems low in the context of the medieval town centre of Cahors. However, these results are specific to the urban morphology and climate studied. It would therefore be interesting to carry out a similar study in other cities.

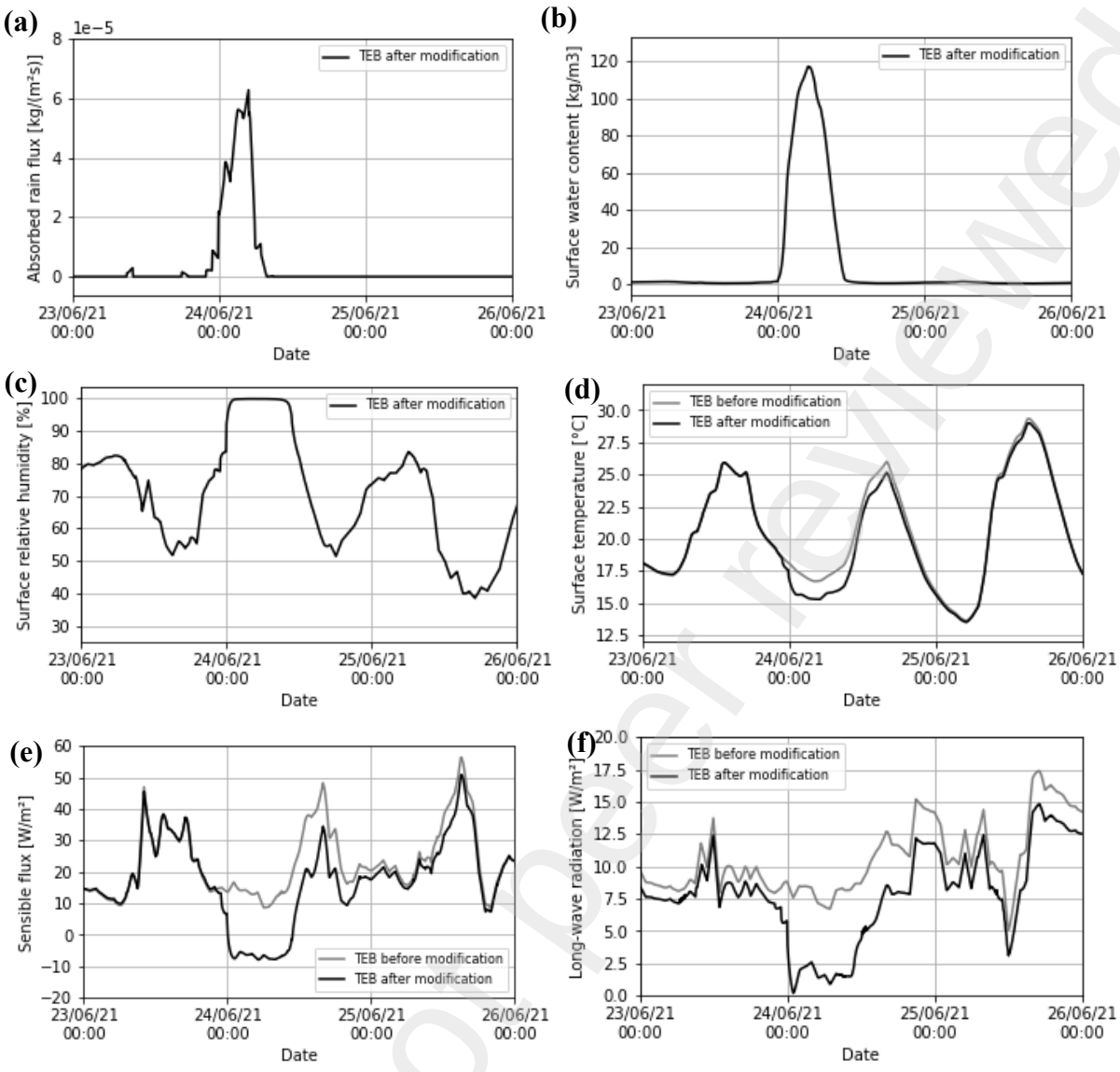

Fig. 14. Behaviour of wall C during the wetting and drying phases: absorbed rainfall (a), surface water content (b), surface relative humidity (c), surface temperature (d), sensible flux (e), and long-wave radiative flux from the surface to the canyon (f).

5. Conclusion

The objective of this paper was to integrate moisture transfer through walls into the urban climate model TEB. For this purpose, a numerical method specially developed to simulate hydric transfer at the urban scale was updated, to improve its numerical stability and to make it easier to integrate into the TEB model. It is based on a decoupled numerical solution approach and an IMEX discretisation scheme. The spatio-temporal discretisation scales are relatively large, to adapt to the urban scale.

The coupled heat and mass transfers have been integrated into the urban climate model TEB by applying the numerical method presented. It was also necessary to add the boundary conditions related to the mass flow, which are dynamically calculated according to the data simulated by TEB in the buildings

and in the urban canyon. New input data have also been introduced to describe the hygrothermal behaviour of materials. This improved version of TEB takes the effect of WDR and the moisture buffering capacity into account. It can thus evaluate the impact of moisture transfers through walls, at the urban scale and under real climatic conditions, over long periods.

This work is based on a case study of the medieval town centre of Cahors. The TEB tool has been configured to simulate this historical district. In this old centre, a building was instrumented, and a weather station installed on a roof. This long-term in situ monitoring was used for the weather forcing of TEB, but also for validation. The results simulated using the TEB model before and after integration of the moisture transfers have been compared to the hygrothermal conditions measured inside a wall and in a building of the medieval neighbourhood. The results simulated with the updated version of TEB are satisfactory at all four points studied (brick/insulation interface, middle of the insulation, inner surface, and indoor conditions). The numerical model and method used to solve the hygrothermal transfers are therefore validated. This also means that the assumptions made to describe the neighbourhood, the walls and the materials of the historical neighbourhood are appropriate.

Both versions of TEB give very satisfactory results for the prediction of indoor and wall temperature. The version after integration of moisture transfers also gives satisfactory results for relative humidity, while the unmodified version of TEB overestimates the amplitude of humidity peaks in the room. The integration of moisture transfer through the walls has therefore greatly improved the prediction of the relative humidity inside the building. On the other hand, moisture transfer through walls and WDR on the façade seem to have little impact on the temperature inside the building, in the wall or in the canyon street.

However, it must not be forgotten that this study was carried out in a particular context of unoccupied buildings. Future work should study these buildings under occupied conditions, with the aim of quantifying the impact of moisture transfer through the walls on occupant comfort and energy consumption. The new version of TEB will also be a powerful tool to evaluate different retrofit scenarios in deserted old centres, such as that of Cahors, taking energy and microclimatic criteria into account. In addition, the new version of the TEB model now simulates the evolution of the hygrothermal conditions in the wall, which will enable the risk of mould growth to be assessed and thus consider a criterion on the wall durability.

This updated version of TEB can also be used to complete the literature on the impact of moisture transfer through walls with different compositions in various climates and urban forms.

Acknowledgements

This work was funded by the University of Toulouse and the Occitanie region of France. The authors would like to thank the town of Cahors for its support and for making the building available to us for testing.

Appendix A: Intermodel validation of the updated method

A numerical validation was performed by comparing the results simulated by the method presented in Section 2 and by the Delphin tool. The methodology applied for the validation was identical to that described in Ruiz et al. (2023). **Table A.1** presents the fifteen wall compositions studied and **Fig. A.1** the results of the validation, which are satisfactory for all cases studied.

Table A.1
Details of the composition of the walls studied (Ruiz et al., 2023).

N°	Composition of the walls from the outside to the inside
1	Brick (0.4 m) – Hemp and lime insulation (0.1 m)
2	Hemp and lime insulation (0.1 m) – Brick (0.4 m)
3	Brick (0.4 m)
4	Hemp and lime insulation (0.1 m)
5	Brick (0.4 m) – Calcium silicate (0.1 m)
6	Brick (0.4 m) – Mineral wool (0.1 m) – Vapour retarder (0.001 m) – Gypsum board (0.01 m)
7	Lime plaster (0.001 m) – Mineral wool (0.1 m) – Brick (0.4 m)
8	Raw earth (0.2 m)
9	Concrete (0.2 m)
10	Mineral fine plaster (0.015 m) – Expanded polystyrene (0.1 m) – Concrete (0.2 m)
11	Concrete (0.2 m) – Mineral wool (0.1 m) – Vapour retarder (0.001 m) – Gypsum board (0.01 m)
12	Old brick (0.215 m)
13	Old brick (0.215 m) – Perforated composite foil (0.001 m) – Phenolic foam (0.05 m) – Composite foil (0.001 m) – Plasterboard (0.0125 m)
14	Old brick (0.215 m) – Glue mortar (0.0065 m) – Calcium silicate (0.14 m) – Lime plaster (0.004 m)
15	Old brick (0.215 m) – Mineral fine plaster (0.008 m) – Wood fibre board (0.1 m) – Gypsum board (0.012 m)

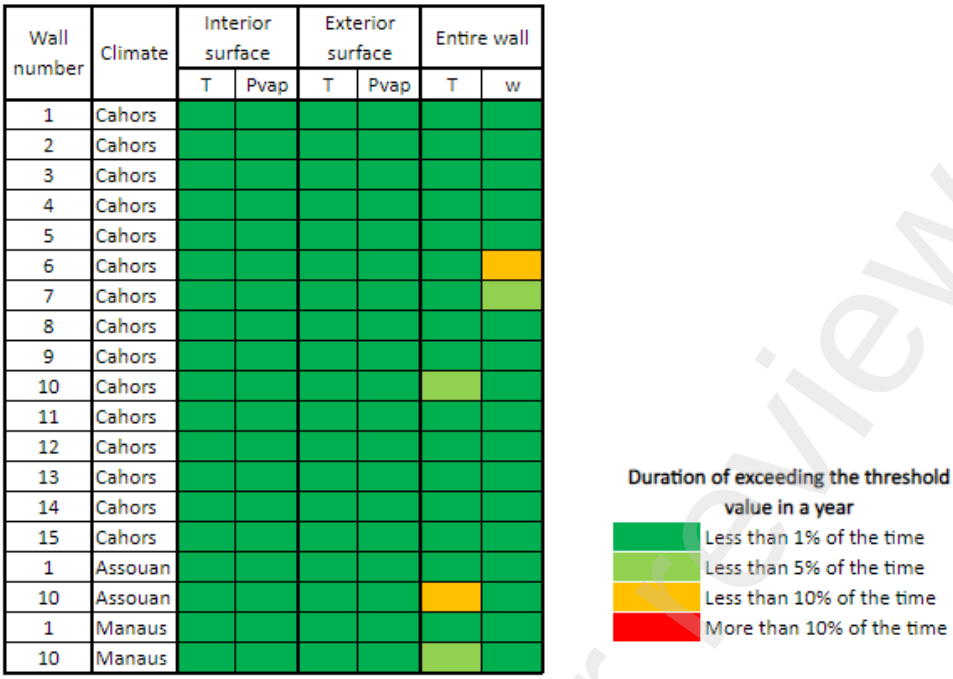

Fig. A.1. Time during which the threshold value was exceeded in a year for each simulation.

Appendix B: Rainfall distribution in the urban canyon

Before moisture transfer through walls was integrated, the TEB tool assumed that rain entering the urban canyon was entirely received by the ground. It was distributed horizontally and uniformly between roads and gardens, regardless of the shape of the urban canyon or wind direction.

Integrating moisture transfer through walls into TEB means adding moisture-related boundary conditions. Each wall can now absorb part of the wind-driven rain. Section 3.4.2.2 details the method for calculating incident rain according to wall orientation, wind speed and direction. Part of the incident rain is absorbed, depending on the current state of the wall, and the remaining incident rain runs off along the wall until it reaches the ground. Note that the absorbed rain is uniformly distributed vertically, as the wall is not discretized.

$$j_{runoff} = j_{rain,inc,wall} - j_{rain,abs,wall} \quad \text{(B.1)}$$

with j_{runoff} runoff along the wall $(kg.m^{-2}.s^{-1})$.

Finally, after the integration of moisture transfer through the walls, the rain received by the ground corresponds to the difference between the rain entering the canyon and the rain absorbed by the building walls (**Fig. B.1**). Rain is still distributed uniformly over the ground, regardless of wind direction.

$$j_{rain,\,ground} = j_{rain} - 0.5(j_{rain,abs,wallA} + j_{rain,abs,wallB}) * r_{wall/ground} \quad \text{(B.2)}$$

with $j_{rain,\,ground}$ rain flux received by the ground (including roads and gardens) $(kg.m^{-2}.s^{-1})$ and $r_{wall/bld}$ wall-to-ground area ratio.

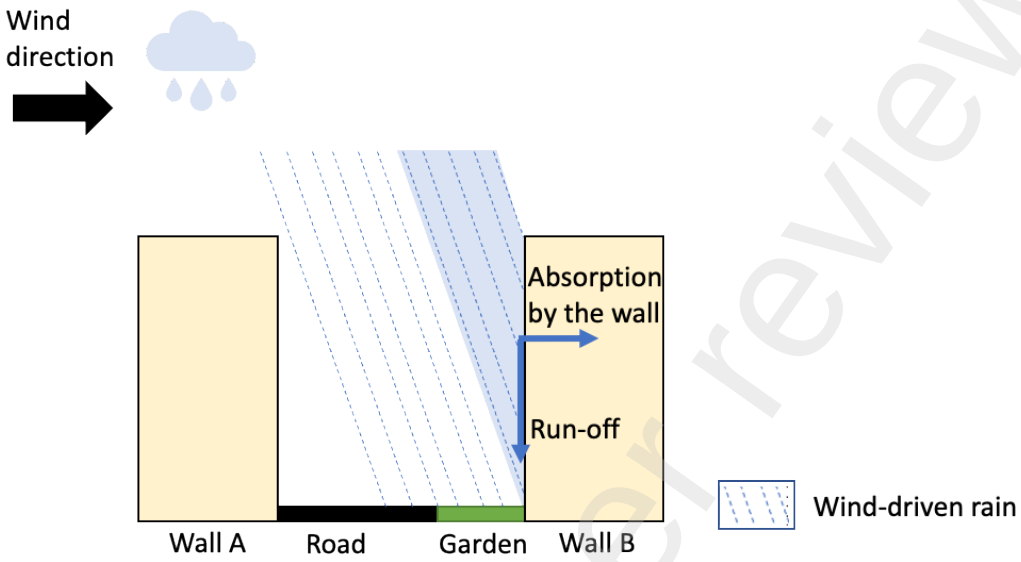

Fig. B.1. Schematic representation of the distribution of driving rain entering the urban canyon.

Appendix C: Hygrothermal properties of wall materials

This appendix presents a detailed version of the hygrothermal characteristics of 16th century brick and hemp-lime that were used to parametrise TEB. These properties are extracted from the characterisation performed by Claude (2018) (**Table C.1**).

Table C.1
Hygrothermal properties of materials.

	Density ρ $(kg.m^{-3})$	**Thermal capacity** C_p $(J.kg^{-1}.K^{-1})$	**Dry thermal conductivity** λ $(W.m^{-1}.K^{-1})$	**Vapour resistance coefficient** μ **(-)**	**Water absorption coefficient** A_w $(kg.m^{-2}.s^{-0.5})$	**Water content at saturation** W_{sat} $(kg.m^{-3})$
16th century brick	1616	800	0.49	9	0.28	388
Hemp and lime insulation	440	1000	0.107	6.5	0.2	789

The moisture retention curve of the brick was described by applying the Durner model. The coefficients used are described in **Table C.2** and the model is unimodal.

Table C.2
Coefficients of Durner model for the brick.

α	m	n	W_{sat} ($kg.m^{-3}$)
2.4553e-5	0.469704	1.88574	386.236

Table C.3 shows the parameters used to describe the evolution of the conductivity of liquid water as a function of water content. The applied model is also unimodal.

Table C.3
Coefficients of Mualem model for the brick.

τ	α	m	n	$K_{l,sat}$ (s)
1	1.22646e-5	0.6915294	3.2418	3.312836e-9

Finally, the water vapour diffusivity of the brick was set to the following value:

$K_v = 1.619\text{e-}11\ kg.m^{-1}.s^{-1}.Pa^{-1}$

For the hemp-lime insulation, the moisture retention curve is described by four points relating capillary pressure to water content (**Table C.4**).

Table C.4
Description of the moisture retention curve for hemp and lime insulation.

P_{cap} ($\log(Pa)$)	θ ($m^3.m^{-3}$)
0	0.789
6.13	0.0324533
8.79	0.00167187
12	0

Similarly, **Table C.5** shows the values used to describe the evolution of liquid conductivity according to water content.

Table C.5
Description of the evolution of liquid conductivity for hemp and lime insulation

θ ($m^3.m^{-3}$)	K_l ($\log(s)$)
0	-25
0.02812959	-14.2068454
0.788	-10.9586953

The vapour diffusion coefficient of hemp-lime was assumed to be constant at the following value:

$K_v = 3.564\text{e-}11\ kg.m^{-1}.s^{-1}.Pa^{-1}$

References

Abuku, M., Blocken, B., Nore, K., Thue, J.V., Carmeliet, J., Roels, S., 2009. On the validity of numerical wind-driven rain simulation on a rectangular low-rise building under various oblique winds. Build. Environ. 44, 621–632. https://doi.org/10.1016/j.buildenv.2008.05.003

Akkurt, G.G., Aste, N., Borderon, J., Buda, A., Calzolari, M., Chung, D., Costanzo, V., Del Pero, C., Evola, G., Huerto-Cardenas, H.E., Leonforte, F., Lo Faro, A., Lucchi, E., Marletta, L., Nocera, F., Pracchi, V., Turhan, C., 2020. Dynamic thermal and hygrometric simulation of historical buildings: Critical factors and possible solutions. Renew. Sustain. Energy Rev. 118, 109509. https://doi.org/10.1016/j.rser.2019.109509

Andreotti, M., Calzolari, M., Davoli, P., Dias Pereira, L., 2022. Hygrothermal performance of an internally insulated masonry wall: Experimentations without a vapour barrier in a historic Italian Palazzo. Energy Build. 260, 111896. https://doi.org/10.1016/j.enbuild.2022.111896

Best, A.C., 1950. The size distribution of raindrops. Q. J. R. Meteorol. Soc. 76, 16–36. https://doi.org/10.1002/qj.49707632704

Blocken, B., Carmeliet, J., 2010. Overview of three state-of-the-art wind-driven rain assessment models and comparison based on model theory. Build. Environ. 45, 691–703. https://doi.org/10.1016/j.buildenv.2009.08.007

Bröde, P., Jendritzky, G., Fiala, D., Havenith, G., 2010. The Universal Thermal Climate Index UTCI in operational use. Presented at the Proceedings of Conference: Adapting to Change: New Thinking on Comfort Cumberland Lodge, Windsor, UK.

Bueno, B., Pigeon, G., Norford, L.K., Zibouche, K., Marchadier, C., 2012. Development and evaluation of a building energy model integrated in the TEB scheme. Geosci. Model Dev. 5, 433–448. https://doi.org/10.5194/gmd-5-433-2012

Camuffo, D., 2019. Microclimate for Cultural Heritage: Measurement, Risk Assessment, Conservation, Restoration, and Maintenance of Indoor and Outdoor Monuments. Elsevier.

Cantin, R., Burgholzer, J., Guarracino, G., Moujalled, B., Tamelikecht, S., Royet, B.G., 2010. Field assessment of thermal behaviour of historical dwellings in France. Build. Environ., 1st International Symposium on Sustainable Healthy Buildings 45, 473–484. https://doi.org/10.1016/j.buildenv.2009.07.010

Carmeliet, J., Blocken, B., Defraeye, T., Derome, D., 2011. Moisture phenomena in whole building performance prediction, in: Building Performance Simulation for Design and Operation. Routledge.

Cassar, M., 2009. Sustainable heritage: challenges and strategies for the twenty-first century. J. Preserv. Technol.

Charrier, A., 2013. Cahors, les chantiers.

Claude, S., 2018. Étude expérimentale et numérique de solutions basées sur les éco-matériaux pour la rénovation thermique du patrimoine bâti urbain (PhD Thesis). INSA de Toulouse.

Claude, S., Ginestet, S., Bonhomme, M., Escadeillas, G., Taylor, J., Marincioni, V., Korolija, I., Altamirano, H., 2019. Evaluating retrofit options in a historical city center: Relevance of bio-based insulation and the need to consider complex urban form in decision-making. Energy Build. 182, 196–204. https://doi.org/10.1016/j.enbuild.2018.10.026

Claude, S., Ginestet, S., Bonhomme, M., Moulène, N., Escadeillas, G., 2017. The Living Lab methodology for complex environments: Insights from the thermal refurbishment of a historical

district in the city of Cahors, France. Energy Res. Soc. Sci., Energy Consumption in Buildings: 32, 121–130. https://doi.org/10.1016/j.erss.2017.01.018

Costa-Carrapiço, I., Croxford, B., Raslan, R., Neila González, J., 2022a. Hygrothermal calibration and validation of vernacular dwellings: A genetic algorithm-based optimisation methodology. J. Build. Eng. 55, 104717. https://doi.org/10.1016/j.jobe.2022.104717

Costa-Carrapiço, I., González, J.N., Raslan, R., Sánchez-Guevara, C., 2022b. Understanding the challenges of determining thermal comfort in vernacular dwellings: A meta-analysis. J. Cult. Herit. 58, 57–73. https://doi.org/10.1016/j.culher.2022.09.019

Dingle, A.N., Lee, Y., 1972. Terminal Fallspeeds of Raindrops. J. Appl. Meteorol. 1962-1982 11, 877–879.

Dorer, V., Allegrini, J., Orehounig, K., Moonen, P., Upadhyay, G., Kämpf, J., Carmeliet, J., 2013. Modelling the urban microclimate and its impact on the energy demand of buildings and building clusters. Proc. BS 2013 13th Conf. Int. Build. Perform. Simul. Assoc. 3483–3489.

Durner, W., 1994. Hydraulic conductivity estimation for soils with heterogeneous pore structure. Water Resour. Res. 30, 211–223. https://doi.org/10.1029/93WR02676

Fechner, H., Ruisinger, U., Nicolai, A., Grunewald, J., 2020. DELPHIN.

Gasparin, S., 2019. Numerical methods for predicting heat and moisture transfer through porous building materials.

Gasparin, S., Berger, J., Dutykh, D., Mendes, N., 2019. An innovative method to determine optimum insulation thickness based on non-uniform adaptive moving grid. J. Braz. Soc. Mech. Sci. Eng. 41, 173. https://doi.org/10.1007/s40430-019-1670-6

Hamdi, R., Masson, V., 2008. Inclusion of a Drag Approach in the Town Energy Balance (TEB) Scheme: Offline 1D Evaluation in a Street Canyon. J. Appl. Meteorol. Climatol. 47, 2627–2644. https://doi.org/10.1175/2008JAMC1865.1

Hansen, T.K., Bjarløv, S.P., Peuhkuri, R.H., Harrestrup, M., 2018. Long term in situ measurements of hygrothermal conditions at critical points in four cases of internally insulated historic solid masonry walls. Energy Build. 172, 235–248. https://doi.org/10.1016/j.enbuild.2018.05.001

Harrestrup, M., Svendsen, S., 2016. Internal insulation applied in heritage multi-storey buildings with wooden beams embedded in solid masonry brick façades. Build. Environ. 99, 59–72. https://doi.org/10.1016/j.buildenv.2016.01.019

Hens, H.L.S.C., 2015. Combined heat, air, moisture modelling: A look back, how, of help? Build. Environ., Fifty Year Anniversary for Building and Environment 91, 138–151. https://doi.org/10.1016/j.buildenv.2015.03.009

Huerto-Cardenas, H.E., Leonforte, F., Aste, N., Del Pero, C., Evola, G., Costanzo, V., Lucchi, E., 2020. Validation of dynamic hygrothermal simulation models for historical buildings: State of the art, research challenges and recommendations. Build. Environ. 180, 107081. https://doi.org/10.1016/j.buildenv.2020.107081

Janssen, H., Blocken, B., Carmeliet, J., 2007. Conservative modelling of the moisture and heat transfer in building components under atmospheric excitation. Int. J. Heat Mass Transf. 50, 1128–1140. https://doi.org/10.1016/j.ijheatmasstransfer.2006.06.048

Janssens, A., Woloszyn, M., Rode, C., Sasic-Kalagasidis, A., De Paepe, M., 2008. From EMPD to CFD – overview of different approaches for Heat Air and Moisture modeling in IEA Annex 41: IEA

ECBCS Annex 41. Proc. IEA ECBCS Annex 41 Closing Semin. 9–20.

Jendritzky, G., Weihs, P., Batchvarova, E., Havenith, G., de Dear, R., 2008. The Universal Thermal Climate Index UTCI Goal and state of COST Action 730 and ISB Commission 6. Presented at the Air Conditioning and the Low Carbon Cooling Challenge, London.

Künzel, H.M., 1995. Simultaneous heat and moisture transport in building components: one- and two-dimensional calculation using simple parameters. IRB Verlag, Stuttgart.

Lawrence Berkeley Laboratory (LBL), 1994. DOE2.1E-053 Source Code.

Maalouf, C., Le, A.D.T., Umurigirwa, S.B., Lachi, M., Douzane, O., 2014. Study of hygrothermal behaviour of a hemp concrete building envelope under summer conditions in France. Energy Build. 77, 48–57. https://doi.org/10.1016/j.enbuild.2014.03.040

Malagoni de Almeida, M., 2022. Etude de la rénovation hygrothermique de parois anciennes utilisant des matériaux biosourcés (PHD Thesis). INSA de Toulouse.

Martin, M., Berdahl, P., 1984. Characteristics of infrared sky radiation in the United States. Sol. Energy 33, 321–336. https://doi.org/10.1016/0038-092X(84)90162-2

Masson, V., 2000. A Physically-Based Scheme For The Urban Energy Budget In Atmospheric Models. Bound.-Layer Meteorol. 94, 357–397. https://doi.org/10.1023/A:1002463829265

Masson, V., Marchadier, C., Bretagne, G., Moine, M.-P., Houet, T., Bonhomme, M., Morel, T., Viguie, V., Avner, P., Aguejdad, R., Briottet, X., Doukari, O., 2013. Projet ACCLIMAT - Adaptation au Changement CLIMatique de l'Agglomération Toulousaine (Research Report).

Masson, V., Pigeon, G., Lemonsu, A., Marchadier, C., Hidalgo, J., Bueno, B., De Munck, C., Daniel, M., Viguie, V., Genovese, E., Salagnac, J.-L., ZIBOUCHE, K., Long, N., Levellier, T., Bonhomme, M., AIT HADDOU, H., Adolphe, L., Nolorgues, L., 2014. Projet MUSCADE, Modélisation Urbaine et Stratégies d'adaptation au Changement Climatique pour Anticiper la Demande et la production Énergétique (Research Report). ANR.

Masson, V., Seity, Y., 2009. Including Atmospheric Layers in Vegetation and Urban Offline Surface Schemes. J. Appl. Meteorol. Climatol. 48, 1377–1397. https://doi.org/10.1175/2009JAMC1866.1

Mendes, N., Winkelmann, F.C., Lamberts, R., Philippi, P.C., 2003. Moisture effects on conduction loads. Energy Build. 35, 631–644. https://doi.org/10.1016/S0378-7788(02)00171-8

Mualem, Y., 1976. A new model for predicting the hydraulic conductivity of unsaturated porous media. Water Resour. Res. 12, 513–522. https://doi.org/10.1029/WR012i003p00513

Nicolai, A., 2007. Modeling and numerical simulation of salt transport and phase transitions in unsaturated porous building materials. Mech. Aerosp. Eng. Theses Diss. https://doi.org/10.13140/RG.2.1.2016.2088

Oke, T.R., 1988. Street design and urban canopy layer climate. Energy Build. 11, 103–113. https://doi.org/10.1016/0378-7788(88)90026-6

Osanyintola, O.F., Simonson, C.J., 2006. Moisture buffering capacity of hygroscopic building materials: Experimental facilities and energy impact. Energy Build. 38, 1270–1282. https://doi.org/10.1016/j.enbuild.2006.03.026

Panico, S., Larcher, M., Marincioni, V., Troi, A., Baglivo, C., Congedo, P.M., 2023. Identifying key parameters through a sensitivity analysis for realistic hygrothermal simulations at wall level supported by monitored data. Build. Environ. 229, 109969. https://doi.org/10.1016/j.buildenv.2022.109969

Priesack, E., Durner, W., 2006. Closed-Form Expression for the Multi-Modal Unsaturated Conductivity Function. Vadose Zone J. 5, 121–124. https://doi.org/10.2136/vzj2005.0066

Roberti, F., Oberegger, U.F., Gasparella, A., 2015. Calibrating historic building energy models to hourly indoor air and surface temperatures: Methodology and case study. Energy Build. 108, 236–243. https://doi.org/10.1016/j.enbuild.2015.09.010

Rode, C., Grau, K., 2003. Whole Building Hygrothermal Simulation Model. ASHRAE Trans. 109.

Rosso, F., Golasi, I., Castaldo, V.L., Piselli, C., Pisello, A.L., Salata, F., Ferrero, M., Cotana, F., de Lieto Vollaro, A., 2018. On the impact of innovative materials on outdoor thermal comfort of pedestrians in historical urban canyons. Renew. Energy 118, 825–839. https://doi.org/10.1016/j.renene.2017.11.074

Rowley, F.B., Algren, A.B., Blackshaw, J.L., 1930. Surface conductances as affected by air velocity, temperature and character of surface. ASHRAE Trans 36, 429–446.

Rowley, F.B., Eckley, W.A., 1932. Surface coefficients as affected by wind direction. ASHRAE Trans 38, 33–46.

Ruiz, M., Masson, V., Bonhomme, M., Ginestet, S., 2023. Numerical method for solving coupled heat and mass transfer through walls for future integration into an urban climate model. Build. Environ. 231, 110028. https://doi.org/10.1016/j.buildenv.2023.110028

Şahin, C.D., Arsan, Z.D., Tunçoku, S.S., Broström, T., Akkurt, G.G., 2015. A transdisciplinary approach on the energy efficient retrofitting of a historic building in the Aegean Region of Turkey. Energy Build. 96, 128–139. https://doi.org/10.1016/j.enbuild.2015.03.018

Saïd, M.N.A., Brown, W.C., Shirtliffe, C.J., Maurenbrecher, A.H.P., 1999. Monitoring of the building envelope of a heritage house: a case study. Energy Build. 30, 211–219. https://doi.org/10.1016/S0378-7788(98)00031-0

Saneinejad, S., Moonen, P., Carmeliet, J., 2014. Coupled CFD, radiation and porous media model for evaluating the micro-climate in an urban environment. J. Wind Eng. Ind. Aerodyn. 128, 1–11. https://doi.org/10.1016/j.jweia.2014.02.005

Saneinejad, S., Moonen, P., Defraeye, T., Derome, D., Carmeliet, J., 2012. Coupled CFD, radiation and porous media transport model for evaluating evaporative cooling in an urban environment. J. Wind Eng. Ind. Aerodyn. 104–106, 455–463. https://doi.org/10.1016/j.jweia.2012.02.006

Sontag, L., Nicolai, A., Vogelsang, S., 2013. Validierung der Solverimplementierung des hygrothermischen Simulationsprogramms Delphin (Technical report).

Straube, J., 2010. Simplified prediction of driving rain on buildings: ASHRAE 160P and WUFI 4.0. Build. Sci. Press 148, 1–16.

Straube, J., Burnett, E., 2000. Simplified prediction of driving rain deposition.

Straube, J., Schumacher, C., 2007. Interior Insulation Retrofits of Load-Bearing Masonry Walls in Cold Climates. J. Green Build. 2, 42–50. https://doi.org/10.3992/jgb.2.2.42

Walton, G.N., 1980. A new algorithm for radiant interchange in room loads calculations. ASHRAE.

Webb, A.L., 2017. Energy retrofits in historic and traditional buildings: A review of problems and methods. Renew. Sustain. Energy Rev. 77, 748–759. https://doi.org/10.1016/j.rser.2017.01.145

Woloszyn, M., Rode, C., 2008. Tools for Performance Simulation of Heat, Air and Moisture Conditions of Whole Buildings. Build. Simul. 1, 5–24. https://doi.org/10.1007/s12273-008-8106-z

Yang, J., Tham, K.W., Lee, S.E., Santamouris, M., Sekhar, C., Cheong, D.K.W., 2017. Anthropogenic heat reduction through retrofitting strategies of campus buildings. Energy Build. 152, 813–822. https://doi.org/10.1016/j.enbuild.2016.11.051

Zhang, M., Qin, M., Rode, C., Chen, Z., 2017. Moisture buffering phenomenon and its impact on building energy consumption. Appl. Therm. Eng. 124, 337–345. https://doi.org/10.1016/j.applthermaleng.2017.05.173

Zhou, X., Carmeliet, J., Sulzer, M., Derome, D., 2020. Energy-efficient mitigation measures for improving indoor thermal comfort during heat waves. Appl. Energy 278, 115620. https://doi.org/10.1016/j.apenergy.2020.115620

Zhou, X., Kubilay, A., Derome, D., Carmeliet, J., 2023. Comparison of wind-driven rain load on building facades in the urban environment and open field: A case study on two buildings in Zurich, Switzerland. Build. Environ. 233, 110038. https://doi.org/10.1016/j.buildenv.2023.110038